

# On the Radio Detectability of Circumplanetary Discs

Zhaohuan Zhu<sup>1\*</sup> Sean M. Andrews<sup>2</sup> and Andrea Isella<sup>3</sup>

<sup>1</sup>*Department of Physics and Astronomy, University of Nevada, Las Vegas, 4505 S. Maryland Pkwy, Las Vegas, NV, 89154, USA*

<sup>2</sup>*Harvard-Smithsonian Center for Astrophysics, 60 Garden Street, Cambridge, MA 02138, USA*

<sup>3</sup>*Department of Physics and Astronomy, Rice University, 6100 Main Street, Houston, TX 77005, USA*

In original form 25 August 2017

## ABSTRACT

Discs around young planets, so-called circumplanetary discs (CPDs), are essential for planet growth, satellite formation, and planet detection. We study the millimetre and centimetre emission from accreting CPDs by using the simple  $\alpha$  disc model. We find that it is easier to detect CPDs at shorter radio wavelengths (e.g.  $\lambda \lesssim 1$  mm). For example, if the system is 140 pc away from us, deep observations (e.g. 5 hours) at ALMA Band 7 (0.87 mm) are sensitive to as small as 0.03 lunar mass of dust in CPDs. If the CPD is around a Jupiter mass planet 20 AU away from the host star and has  $\alpha \lesssim 0.001$ , ALMA can detect this disc when it accretes faster than  $10^{-10} M_{\odot}/yr$ . ALMA can also detect the “minimum mass sub-nebulae” disc if such a disc exists around a young planet in YSOs. However, to distinguish the embedded compact CPD from the circumstellar disc material, we should observe circumstellar discs with large gaps/cavities using the highest resolution possible. We also calculate the CPD fluxes at VLA bands, and discuss the possibility of detecting radio emission from jets/winds launched in CPDs. Finally we argue that, if the radial drift of dust particles is considered, the drifting timescale for millimetre dust in CPDs can be extremely short. It only takes  $10^2$ - $10^3$  years for CPDs to lose millimetre dust. Thus, for CPDs to be detectable at radio wavelengths, mm-sized dust in CPDs needs to be replenished continuously, or the disc has a significant fraction of micron-sized dust or a high gas surface density so that the particle drifting timescale is long, or the radial drift is prevented by other means (e.g. pressure traps).

**Key words:** radiation mechanisms: thermal — planets and satellites: detection — planet-disc interactions — protoplanetary discs — brown dwarfs — radio continuum: planetary systems — submillimetre: planetary systems

## 1 INTRODUCTION

During their formation, giant planets are expected to be surrounded by dense discs made of gas and dust called circumplanetary discs (CPDs). The orbital properties of regular satellites around giant planets in our solar system support the existence of CPDs in the past. All medium and large satellites of giant planets in our solar systems, except the captured satellite Triton, have prograde orbits that are nearly coplanar with the planet’s equator. Furthermore, the gradient in the amount of ices in the Galilean satellites is consistent with satellite formation in a warm disc.

Theoretical studies suggest that, after the runaway phase of giant planet formation, the planet’s atmosphere detaches from the planet’s Hill sphere and shrinks significantly (Papaloizou & Nelson 2005). Material that falls into the planet’s Hill sphere will spin around the planet, forming CPDs to conserve the angular momentum (Lubow et al. 1999; Ayliffe & Bate 2009; Szulágyi et al. 2016). The planet

can continue to grow with material being accreted through the CPDs.

Studying CPDs is crucial for understanding satellite formation, and even habitability of life on satellites (e.g. Europa and Enceladus, Waite et al. 2017). The density and temperature structure of CPDs affect the satellite size and composition. If the CPD is too hot for water to condense, the satellites will be made mostly of dust grains with little sub-surface water ocean (Canup & Ward 2002). Forming large satellites and multiple satellites in resonance (e.g. Galilean satellites) can lead to geological activity, providing energy sources for early life (Peale 1999).

Despite their importance, finding CPDs in other young stellar objects (YSOs) is challenging since these discs are a lot fainter than the central star. On the other hand, when CPDs are actively accreting, they can be as bright as a late M-type/early L-type brown dwarf (Quillen & Trilling 1998; Zhu 2015). Unlike the SEDs of a brown dwarf, the SEDs of accreting CPDs are a lot redder, peaking at mid-infrared. Thus, to detect CPDs in protostellar systems, we need to image the young stellar system at mid-infrared,

\* E-mail: zhaohuan.zhu@unlv.edu

adopting high contrast imaging techniques capable of blocking most of the stellar light. With such observational strategy, a few red sources within circumstellar discs have been discovered (LkCa 15b: Kraus & Ireland 2012, HD100546b: Quanz et al. 2013; Currie et al. 2015, but see Rameau et al. 2017, HD169142b: Biller et al. 2014; Reggiani et al. 2014) and their photometries at infrared bands are consistent with accreting CPDs (Zhu 2015; Zhu et al. 2016). Besides the photometry, another observational signature of accretion discs is  $H_\alpha$  emission lines (Calvet & Gullbring 1998; Muzerolle et al. 1998, 2001; Zhou et al. 2014). So far, LkCa 15b is the most promising candidate for the accreting CPDs since both the accretion indicators,  $H_\alpha$  line and near-IR thermal emission, have been detected (Sallum et al. 2015).

Besides optical and infrared observations, radio observations can potentially detect the CPDs too. Using the parameterized models, Isella et al. (2014) suggests that ALMA can detect CPDs with mass down to  $5 \times 10^{-4} M_J$  and size down to 0.2 AU. With numerical simulations, Zhu et al. (2016) suggests that the central star can induce spiral shocks in CPDs and the dissipation of the shocks can lead to CPD accretion. Applying this accretion disc model to the CPD candidates mentioned above (HD100546b, HD169142b, LkCa 15b), all these CPD candidates should be detectable by ALMA (Zhu et al. 2016). In this paper, we extend Isella et al. (2014) with detailed disc vertical structure calculations to show whether CPDs can be detected by ALMA and future generation radio telescopes such as the Next Generation VLA (ngVLA, Selina & Murphy 2017). In §2, we introduce the analytical disc model. The results are presented in §3. Finally, after short discussions in §4, the paper is summarized in §5.

## 2 METHOD

To calculate the radio emission from CPDs, we first need to construct a disc model. Following the  $\alpha$  disc theory, and similarly to circumstellar discs (D’Alessio et al. 1998), the structure of a CPD is determined by the disc accretion rate ( $\dot{M}_p$ ), the viscosity parameter ( $\alpha$ ), and the disc inner and outer radius ( $R_{in}$ ,  $R_{out}$ ), as long as the planet mass ( $M_p$ ), temperature ( $T_p$ ), and radius ( $R_p$ ) are given. Unfortunately, we don’t have much, if any, observational constraints on these parameters. Thus, we narrow down the parameter space using either order-of-magnitude estimates or theoretical results from numerical calculations.

To form a Jupiter mass planet within the lifetime of the gaseous circumstellar discs ( $\sim 10^6$  yrs), the average CPD accretion rate ( $\dot{M}_p$ ) is  $10^{-6} M_J/\text{yr}$ . In this paper, we vary  $M_p \dot{M}_p$  from  $10^{-5} M_J^2/\text{yr}$  to  $10^{-8} M_J^2/\text{yr}$ . We choose  $M_p \dot{M}_p$  as a fundamental parameter since  $M_p \dot{M}_p$  determines the disc effective temperature for a viscous heating dominated disc (Equation 1). However, for the radio emission calculation,  $M_p$  and  $\dot{M}_p$  become degenerate when the disc is optically thin or irradiation dominated (§3.1, 3.2, 4.1). Thus, we normally also specify  $M_p$  whenever  $M_p \dot{M}_p$  is given.

Another important parameter for determining the disc structure is the viscosity coefficient:  $\alpha$  parameter. The first-principle hydrodynamical simulations by Zhu et al. (2016) suggest that spiral shocks induced by the star can lead to efficient angular momentum transport in CPDs. In this accretion scenario, the value of  $\alpha$  parameter depends on the disc accretion rate due to the thermal feedback. For a disc

accreting at a higher rate, the disc is hotter, leading to more-opened spiral shocks so that the shock-driven accretion is more efficient with a higher  $\alpha$ . Over a wide range of accretion rates ( $\dot{M}_p$  from  $10^{-12} M_\odot/\text{yr}$  to  $10^{-8} M_\odot/\text{yr}$ ),  $\alpha$  can vary from 0.0001 to 0.1.

The disc inner radius is assumed to be the Jupiter radius ( $R_J$ ), and the outer radius of the CPD ( $R_{out}$ ) is assumed to be 1/3 of the Hill radius of the planet (Quillen & Trilling 1998; Martin & Lubow 2011), or  $R_{out} = 1/3 \times r_p (M_p/3M_*)^{1/3}$ . In this paper, we use  $R$  to represent the radius in the circumplanetary disc (the distance to the planet), and  $r$  to represent the radius in the circumstellar disc (the distance to the central star). For a Jupiter mass planet at  $r_p=5, 20,$  and  $80$  AU from the solar mass star,  $R_{out}$  is 0.12, 0.46, and 1.85 AU.

With these disc parameters ( $\dot{M}_p$ ,  $\alpha$ ,  $R_{in}$ , and  $R_{out}$ ), we can calculate the disc structure by solving coupled radiative transfer and hydrostatic equilibrium equations as in D’Alessio et al. (1996). However, such detailed CPD models are not necessary at the current stage where these parameters are still highly uncertain. Thus in this paper, we make approximations to simplify the calculations.

Given the  $M_p \dot{M}_p$ , the viscous theory suggests that the disc effective temperature follows

$$T_{eff}^4 = \frac{3GM_p \dot{M}_p}{8\pi\sigma R^3} \left[ 1 - \left( \frac{R_{in}}{R} \right)^{1/2} \right], \quad (1)$$

where  $R_{in}$  is the disc inner radius and we assume  $R_{in} = 0.1R_\odot \sim R_J$ . To derive the disc midplane temperature, we assume that the disc vertical temperature along the height ( $z$ ) follows Hubeny (1990),

$$T(z)^4 = \frac{3}{8} T_{eff}^4 \tau_R + T_{ext}^4, \quad (2)$$

where  $\tau_R$  is the Rosseland mean optical depth at  $z$ , and  $T_{ext}$  is the background temperature due to the external irradiation. Here we include both the heating from ISM and the irradiation from the planet as  $T_{ext}^4 = T_{ISM}^4 + T_{irr}^4$ . We choose  $T_{ISM} = 10$  K and assume that  $T_{irr}$  could be due to the radiation from either the central bright planet or the disc boundary layer<sup>1</sup>. The planet or the boundary layer will irradiate the disc at a large incident angle. The incident angle is  $\tan^{-1}(H/R)$  to the first order (Kenyon & Hartmann 1987). With  $H/R \sim 0.1$  (Zhu et al. 2016), we assume that the disc receives 1/10th of the irradiated energy in the direction perpendicular to the disc surface. Thus,

$$T_{irr} = \left( \frac{L_{irr}}{\sigma 40\pi R^2} \right)^{1/4}. \quad (3)$$

When we consider the irradiation from a bright planet, we assign  $L_{irr}$  based on the “hot start” planet model (e.g. Marley et al. 2007; Spiegel & Burrows 2012). When we consider the irradiation from the boundary layer, we adopt  $L_{irr} = GM_p \dot{M}_p / (2R_p)$  since half of the accretion energy is released at the boundary layer.

<sup>1</sup> We have ignored the irradiation from the protoplanetary disc and the central star. Such irradiation can be important if the planet is close to the central star (e.g. 5 AU, see discussion in §4.1). On the other hand, as shown in §3.2 and §4.1, irradiation makes little difference on the radio emission.

The disc midplane temperature is then

$$T_c^4 = \frac{9GM_p\dot{M}_p\Sigma\kappa_R}{128\pi\sigma R^3} \left[ 1 - \left( \frac{R_{in}}{R} \right)^{1/2} \right] + T_{ext}^4, \quad (4)$$

where  $\kappa_R$  is the Rosseland mean opacity and we choose the nominal value of  $\kappa_R = 10 \text{ cm}^2/\text{g}$ .

Using the viscous disc theory, we also have

$$\nu\Sigma = \frac{\dot{M}}{3\pi} \left[ 1 - \left( \frac{R_{in}}{R} \right)^{1/2} \right], \quad (5)$$

where  $\nu = \alpha c_{s,iso}^2/\Omega$  in the  $\alpha$  disc model.

With Equations 1-5, we can solve  $\Sigma$  numerically. On the other hand, we can also approximate the solution with analytical formulae in the following way. First, if we ignore  $T_{ext}$ , we can solve  $\Sigma$  analytically as

$$\Sigma = \frac{27^{7/5}}{3^{6/5}} \left( \frac{\sigma GM_p \dot{M}_p^3}{\alpha^4 \pi^3 \kappa_R R^3} \right)^{1/5} \left( \frac{\mu}{\mathfrak{R}} \right)^{4/5} \left[ 1 - \left( \frac{R_{in}}{R} \right)^{1/2} \right]^{3/5}, \quad (6)$$

where  $\mu$  and  $\mathfrak{R}$  are the mean molecular weight and the gas constant. Considering the disc is mostly cold, we choose  $\mu = 2.4$ . On the other hand, if we ignore the viscous heating and assume  $T_c$  is dominated by  $T_{ext}$ , we can solve  $\Sigma$  as

$$\Sigma = \frac{\dot{M}_P \mu \Omega}{3\pi \alpha \mathfrak{R} T_{ext}}. \quad (7)$$

In reality, both viscous heating and external irradiation contribute to  $T_c$ , and a larger  $T_c$  will result in a smaller  $\Sigma$  (Equation 5). Thus, we choose  $\Sigma$  as the minimum of  $\Sigma$  derived from Equations 6 and 7. With the  $\Sigma$  determined, we can calculate the midplane temperature using Equation 4.

Knowing the disc surface density and the vertical temperature structure (Equation 2), we can finally calculate the disc radio continuum emission. First, we calculate the disc's optical depth at the given radio wavelength ( $\tau_{mm} = \kappa_{mm}\Sigma/2$ ). Although the disc is normally optically thick with the Rosseland mean opacity, it can be optically thin at millimetre (mm) and centimetre (cm) considering the significantly lower dust opacity at the radio wavelength range. We adopt the mass opacity from Andrews et al. (2012),  $\kappa_{mm} = 0.034 \times (0.87\text{mm}/\lambda) \text{ cm}^2/\text{g}$  which assumes a dust-to-gas mass ratio of 0.01. When the disc is optically thick at mm, the disc's effective brightness temperature at mm ( $T_b$ )<sup>2</sup> will equal the disc's temperature at  $\tau_{mm}(z) = 1$ . When the disc is optically thin at mm, we can calculate the effective brightness temperature by integrating the product of the temperature, opacity, and density along the disc height. Considering most of the disc mass is at the midplane and most radio emission comes from the material at the midplane in the optically thin limit, the effective brightness temperature is then simply the disc's midplane temperature weighted by the disc optical depth.

<sup>2</sup> In this paper, we define the effective brightness temperature as the equivalent temperature a black body would have in order to be as bright as the observed brightness, to be distinguished from the brightness temperature used in the radio literature which refers to the equivalent temperature measured within one observational beam.

Thus,

$$T_b = \begin{cases} \left( \frac{3}{8} \frac{\kappa_R}{\kappa_{mm}} T_{eff}^4 + T_{ext}^4 \right)^{1/4} & \text{if } \tau_{mm} > 0.5 \\ 2T_c\tau_{mm} & \text{if } \tau_{mm} < 0.5 \end{cases} \quad (8)$$

where  $\tau_{mm} = 0.5\Sigma\kappa_{mm}$ . Then, we can calculate the flux emitted at every disc radius, using  $I = 2kT_b/\lambda^2$ . After integrating the whole disc, the total CPD emission at mm is derived. We want to caution that, by using the opacity law above and applying the same opacity law throughout the disc, we assume that the dust-to-gas mass ratio is 1/100 and the dust is perfectly coupled to the gas. As shown in §4.6, the perfect coupling is only correct for micron sized particles. If particles are large enough to decouple from the gas, we could have dramatically different conclusions (§4.6).

we can also calculate the averaged effective brightness temperature at mm over the whole CPD surface,

$$\overline{T_b} = \frac{\int_{R_{in}}^{R_{out}} T_b 2\pi R dR}{\pi R_{out}^2}. \quad (9)$$

This averaged effective brightness temperature can be compared with the brightness temperature limit of the telescope to estimate if the disc is detectable by ALMA or ngVLA. For example, let's assume 1-hour ALMA band 7 observation has a 0.7 K noise level, and the desired observational beam size is 0.03". And we want to observe a CPD which is 20 AU from the central star and 140 pc away from us. The angular size of the CPD will be 0.006", which will be smaller than the observational beam by a factor of 5. We also know that the predicted averaged effective brightness temperature for this CPD is 380 K from Table 1. Then, the brightness temperature received by one observational beam will be  $380/5^2 = 15.2$  K, and we can get a S/N =  $(15.2/0.7) = 22$  detection with 1-hour integration.

Tables 1 and 2 summarize the fluxes and the averaged effective brightness temperatures for all our cases when the source is 140 pc away (e.g. in the Taurus star forming region). The planet mass is assumed to be 1  $M_J$  in Table 1, and 1  $M_J$  or 10  $M_J$  in Table 2. Table 1 shows the discs in the viscous limit, which means that the planet is faint (e.g. it had a "cold start") and the viscous heating determines the disc temperature structure. For such viscous discs, the disc's effective temperature only depends on the product of  $M_p$  and  $\dot{M}_p$  (Equation 1), and, when the disc is optically thick at mm, the mm emission will only depend on  $M_p\dot{M}_p$ . Thus, we use  $M_p\dot{M}_p$ ,  $\alpha$ , and  $R_{out}$  as three fundamental parameters. However, when the disc is optically thin or is irradiated by the bright planet, the flux will also depend on  $M_p$  (Equations 6 and 7, more discussion in §3.2, and 4.1).

In Table 1, under each temperature and flux column, there are two sub-columns: "b." refers to the cases which consider the boundary layer irradiation ( $L_{irr} = L_{acc} = GM_p\dot{M}_p/(2R_{in})$ ), and "no b." refers to the cases without considering the boundary layer irradiation.

Table 2 shows the cases where the planet is bright (e.g. the planet has a "hot start") and the irradiation from the central planet to the disc is important for determining the disc temperature. Three planet luminosities ( $L_{irr} = 10^{-3}, 10^{-4}, 10^{-5} L_\odot$ ) have been considered. In Table 2, we list results with both  $M_p = 1M_J$  and  $M_p = 10M_J$ . Notice that with  $M_p = 10M_J$ , the disc with  $R_{out} = 0.48AU$

**Table 1.** Viscous Discs with  $M_p = 1M_J$ . The left three columns are input parameters, while other columns are derived quantities.

$M_p \dot{M}_p$ $M_J^2/\text{yr}$	$\alpha$	$R_{out}$ AU	$\dot{M}_{disc}$ $M_J$	$L$ $10^{-3}L_\odot$	F(0.85mm)		F(1.3mm)		F(3mm)		F(10mm)		$\overline{T}_b(0.85mm)$		$\overline{T}_b(1.3mm)$		$\overline{T}_b(3mm)$		$\overline{T}_b(10mm)$	
					$\mu\text{Jy}$ no b.	$\mu\text{Jy}$ b.	K no b.	K b.	K no b.	K b.	K no b.	K b.	K no b.	K b.						
1e-5	1e-1	0.12	8.7e-5	1.570	4.2e1	4.3e1	1.3e1	1.3e1	1.2	1.2	3.3e-2	3.3e-2	219	225	159	163	76	78	24	24
1e-5	1e-2	0.12	5.5e-4	1.570	7.3e1	7.4e1	3.5e1	3.5e1	7.3	7.4	3.0e-1	3.0e-1	380	384	422	425	475	477	213	214
1e-5	1e-3	0.12	3.5e-3	1.570	7.3e1	7.4e1	3.5e1	3.5e1	8.0	8.1	9.8e-1	9.8e-1	380	384	422	425	520	522	703	704
1e-5	1e-4	0.12	2.2e-2	1.570	7.3e1	7.4e1	3.5e1	3.5e1	8.0	8.1	9.8e-1	9.8e-1	380	384	422	425	520	522	703	704
1e-5	1e-1	0.46	6.1e-4	1.570	1.0e2	1.2e2	3.0e1	3.4e1	2.5	2.9	7.0e-2	7.9e-2	33	38	23	26	10	12	3	4
1e-5	1e-2	0.46	3.8e-3	1.570	4.2e2	4.4e2	1.8e2	1.9e2	2.1e1	2.2e1	6.7e-1	6.9e-1	136	142	140	145	85	88	30	31
1e-5	1e-3	0.46	2.4e-2	1.570	4.2e2	4.4e2	2.0e2	2.0e2	4.6e1	4.7e1	4.5	4.6	136	142	151	155	186	189	204	205
1e-5	1e-4	0.46	1.5e-1	1.570	4.2e2	4.4e2	2.0e2	2.0e2	4.6e1	4.7e1	5.6	5.6	136	142	151	155	186	189	252	253
1e-5	1e-1	1.85	4.2e-3	1.570	2.3e2	2.9e2	6.4e1	8.2e1	5.3	6.8	1.5e-1	1.9e-1	4.57	5.90	3.05	3.92	1.35	1.73	0.41	0.52
1e-5	1e-2	1.85	2.7e-2	1.570	1.6e3	2.0e3	5.2e2	6.3e2	4.9e1	5.7e1	1.4	1.6	33	40	25	30	12	14	4	5
1e-5	1e-3	1.85	1.7e-1	1.570	2.4e3	2.7e3	1.1e3	1.2e3	2.6e2	2.7e2	1.2e1	1.3e1	48	55	54	59	66	69	34	35
1e-5	1e-4	1.85	1.1	1.570	2.4e3	2.7e3	1.1e3	1.2e3	2.6e2	2.7e2	3.2e1	3.2e1	48	55	54	59	66	69	90	91
1e-6	1e-1	0.12	2.2e-5	0.157	5.2	5.6	1.5	1.6	1.2e-1	1.3e-1	3.3e-3	3.5e-3	27	29	18	19	8	8	2	3
1e-6	1e-2	0.12	1.4e-4	0.157	3.5e1	3.6e1	1.2e1	1.2e1	1.1	1.1	3.3e-2	3.3e-2	181	185	142	144	73	74	23	24
1e-6	1e-3	0.12	8.7e-4	0.157	4.1e1	4.2e1	2.0e1	2.0e1	4.5	4.5	2.7e-1	2.7e-1	213	216	237	239	293	293	195	195
1e-6	1e-4	0.12	5.5e-3	0.157	4.1e1	4.2e1	2.0e1	2.0e1	4.5	4.5	5.5e-1	5.5e-1	213	216	237	239	293	293	395	396
1e-6	1e-1	0.46	1.5e-4	0.157	1.1e1	1.4e1	3.2	4.0	2.6e-1	3.2e-1	7.0e-3	8.7e-3	3.65	4.58	2.41	3.01	1.05	1.31	0.31	0.39
1e-6	1e-2	0.46	9.6e-4	0.157	9.5e1	1.1e2	2.8e1	3.1e1	2.5	2.7	7.0e-2	7.6e-2	31	34	22	24	10	11	3	3
1e-6	1e-3	0.46	6.1e-3	0.157	2.4e2	2.5e2	1.1e2	1.2e2	1.8e1	1.9e1	6.4e-1	6.5e-1	77	80	85	87	74	76	29	29
1e-6	1e-4	0.46	3.8e-2	0.157	2.4e2	2.5e2	1.1e2	1.2e2	2.6e1	2.6e1	3.2	3.2	77	80	85	87	105	106	142	142
1e-6	1e-1	1.85	1.1e-3	0.157	2.7e1	3.1e1	7.5	8.8	6.1e-1	7.1e-1	1.6e-2	1.9e-2	0.54	0.63	0.36	0.42	0.15	0.18	0.05	0.05
1e-6	1e-2	1.85	6.7e-3	0.157	2.2e2	2.8e2	6.5e1	8.0e1	5.4	6.7	1.5e-1	1.8e-1	4.56	5.66	3.07	3.79	1.38	1.69	0.42	0.51
1e-6	1e-3	1.85	4.2e-2	0.157	1.3e3	1.5e3	4.5e2	5.2e2	4.6e1	5.2e1	1.4	1.6	26	30	22	25	12	13	4	4
1e-6	1e-4	1.85	2.7e-1	0.157	1.3e3	1.5e3	4.5e2	5.2e2	1.5e2	1.5e2	1.1e1	1.1e1	27	31	30	33	37	39	30	31
1e-7	1e-1	0.12	5.5e-6	0.016	5.3e-1	6.4e-1	1.5e-1	1.8e-1	1.2e-2	1.5e-2	3.3e-4	3.9e-4	2.77	3.34	1.81	2.18	0.78	0.95	0.24	0.28
1e-7	1e-2	0.12	3.2e-5	0.016	5.0	5.3	1.5	1.5	1.2e-1	1.3e-1	3.3e-3	3.4e-3	26	27	18	19	8	8	2	2
1e-7	1e-3	0.12	2.5e-4	0.016	2.3e1	2.3e1	9.6	9.7	1.0	1.1	3.2e-2	3.3e-2	120	121	116	117	68	68	23	23
1e-7	1e-4	0.12	1.4e-3	0.016	2.3e1	2.3e1	1.1e1	1.1e1	2.5	2.5	2.3e-1	2.3e-1	120	121	133	134	165	165	167	167
1e-7	1e-1	0.46	3.8e-5	0.016	1.2	1.5	3.4e-1	4.2e-1	2.7e-2	3.4e-2	7.4e-4	9.2e-4	0.39	0.49	0.26	0.32	0.11	0.14	0.03	0.04
1e-7	1e-2	0.46	2.4e-4	0.016	1.1e1	1.4e1	3.2	3.8	2.6e-1	3.2e-1	7.0e-3	8.5e-3	3.63	4.41	2.41	2.92	1.06	1.28	0.32	0.38
1e-7	1e-3	0.46	1.5e-3	0.016	8.4e1	9.1e1	2.6e1	2.8e1	2.4	2.6	6.9e-2	7.4e-2	27	29	20	22	10	10	3	3
1e-7	1e-4	0.46	9.6e-3	0.016	1.3e2	1.4e2	6.3e1	6.5e1	1.4e1	1.4e1	6.0e-1	6.1e-1	43	45	48	49	57	58	27	27
1e-7	1e-1	1.85	1.6e-4	0.016	2.9	3.2	8.1e-1	8.9e-1	6.6e-2	7.3e-2	1.8e-3	2.0e-3	0.06	0.06	0.04	0.04	0.02	0.02	0.01	0.01
1e-7	1e-2	1.85	1.3e-3	0.016	2.8e1	3.1e1	7.8	8.6	6.4e-1	7.0e-1	1.7e-2	1.9e-2	0.56	0.62	0.37	0.41	0.16	0.18	0.05	0.05
1e-7	1e-3	1.85	1.0e-2	0.016	2.3e2	2.6e2	6.8e1	7.6e1	5.8	6.4	1.6e-1	1.8e-1	4.74	5.28	3.24	3.60	1.47	1.63	0.45	0.50
1e-7	1e-4	1.85	6.7e-2	0.016	8.0e2	8.8e2	3.6e2	3.9e2	4.4e1	4.7e1	1.4	1.5	16.24	17.94	17.26	18.72	11.02	11.91	3.93	4.21
1e-8	1e-1	0.12	1.4e-6	0.002	5.4e-2	7.0e-2	1.5e-2	2.0e-2	1.2e-3	1.6e-3	3.3e-5	4.3e-5	0.28	0.36	0.19	0.24	0.08	0.10	0.02	0.03
1e-8	1e-2	0.12	8.7e-6	0.002	5.4e-1	6.2e-1	1.5e-1	1.7e-1	1.2e-2	1.4e-2	3.3e-4	3.8e-4	2.78	3.20	1.82	2.09	0.79	0.91	0.24	0.27
1e-8	1e-3	0.12	5.5e-5	0.002	4.7	4.9	1.4	1.4	1.2e-1	1.2e-1	3.3e-3	3.4e-3	24.46	25.37	16.98	17.58	7.78	8.04	2.35	2.43
1e-8	1e-4	0.12	3.5e-4	0.002	1.3e1	1.3e1	6.2	6.2	9.2e-1	9.3e-1	3.1e-2	3.1e-2	67.51	68.27	75.07	75.62	59.84	60.27	22.51	22.65
1e-8	1e-1	0.46	7.0e-6	0.002	1.4e-1	1.5e-1	3.9e-2	4.3e-2	3.1e-3	3.5e-3	8.5e-5	9.5e-5	0.04	0.05	0.03	0.03	0.01	0.01	0.00	0.00
1e-8	1e-2	0.46	5.6e-5	0.002	1.3	1.5	3.7e-1	4.1e-1	3.0e-2	3.4e-2	8.0e-4	9.1e-4	0.42	0.48	0.28	0.31	0.12	0.14	0.04	0.04
1e-8	1e-3	0.46	3.8e-4	0.002	1.1e1	1.3e1	3.3	3.7	2.7e-1	3.1e-1	7.4e-3	8.3e-3	3.70	4.18	2.48	2.80	1.10	1.24	0.33	0.37
1e-8	1e-4	0.46	2.4e-3	0.002	6.9e1	7.2e1	2.4e1	2.5e1	2.3	2.4	6.9e-2	7.2e-2	22.25	23.37	17.88	18.76	9.39	9.80	3.10	3.23
1e-8	1e-1	1.85	1.9e-5	0.002	3.1e-1	3.2e-1	8.6e-2	9.1e-2	7.0e-3	7.4e-3	1.9e-4	2.0e-4	0.01	0.01	0.00	0.00	0.00	0.00	0.00	0.00
1e-8	1e-2	1.85	1.8e-4	0.002	3.0	3.2	8.4e-1	8.9e-1	6.8e-2	7.2e-2	1.8e-3	1.9e-3	0.06	0.06	0.04	0.04	0.02	0.02	0.01	0.01
1e-8	1e-3	1.85	1.6e-3	0.002	2.8e1	3.0e1	8.0	8.4	6.6e-1	6.9e-1	1.8e-2	1.9e-2	0.58	0.61	0.38	0.40	0.17	0.18	0.05	0.05
1e-8	1e-4	1.85	1.3e-2	0.002	2.3e2	2.4e2	6.9e1	7.2e1	6.1	6.3	1.7e-1	1.8e-1	4.72	4.89	3.30	3.42	1.53	1.59	0.48	0.49

corresponds to a CPD at 9.3 AU instead of 20 AU. When the irradiation is weak (e.g.  $L_p = 10^{-5}L_\odot$ ), viscous heating dominates and the flux of CPDs with  $M_p = 1M_J$  in Table 2 is similar to those in Table 1.

### 3 RESULTS

In §3.1, we first present the results without including the irradiation from the planet to the disc (cases in Table 1). Then, in §3.2, we present the results which consider the planet irradiation (cases in Table 2).

#### 3.1 Viscous Heating Dominated Discs

Without the planet irradiation, the disc thermal structure is solely determined by the viscous accretion. The disc structure for CPDs with  $\dot{M}_p = 10^{-5} M_J/\text{yr}$  and  $M_p = 1M_J$  is shown in Figure 1. Two cases with different  $\alpha$  values ( $\alpha = 0.01$  and  $0.001$ ) are presented. The disc surface density follows  $R^{-3/5}$ , as in Equation 6. With a smaller  $\alpha$  (upper panels), the disc surface density is higher in order to maintain the same accretion rate. Since this disc is almost optically thick at mm within 2 AU, the effective brightness temperature at mm is always higher than the effective temperature calculated with the Rosseland mean opacity. With a higher  $\alpha$  (lower panels), the surface density is lower and

the outer disc becomes optically thin at mm, so that the brightness temperature drops off faster there.

The figure also suggests that the midplane temperature at the very inner disc ( $< 0.03$  AU or  $60 R_J$ ) can be higher than the dust sublimation temperature ( $\sim 1500$  K). Dust will sublimate at the inner disc and the disc will be ionized. The ionized plasma at the inner disc can also radiate at mm from free-free emission. For example, at 100 GHz our sun's brightness temperature ( $\sim 7000$  K) is similar to the temperature of the photosphere. Thus, we simply assume that the brightness temperature from the free-free emission at the inner disc is the same as the brightness temperature calculated using dust opacity. Furthermore, as we will show in §4.1, most of the radio emission comes from the outer disc, and changing the inner radius from  $R_J$  to  $100 R_J$  has little effect on the radio emission.

With the effective brightness temperature known, we can calculate the flux at each radius and integrate the total flux in the disc. Figure 2 shows the integrated flux as a function of the disc outer radius  $R_{out}$ . The solid curves are for the case shown in the upper panels of Figure 1 having a lower  $\alpha$  value, while the dashed curves are for the case shown in the bottom panels of Figure 1 having a higher  $\alpha$  value. The vertical dotted lines label the three different disc sizes  $R_{out} = 0.12, 0.46,$  and  $1.85$  AU, which correspond to a CPD around a Jupiter mass planet at 5, 20, 80 AU from the central solar mass star. As clearly demonstrated in Figure 2, when the disc is optically thick at a particular wavelength,

**Table 2.** Irradiated Discs. The values of  $10^{-5}$ ,  $10^{-4}$ ,  $10^{-3}$  in the third row refer to cases with  $L_{irr} = 10^{-5}L_{\odot}$ ,  $10^{-4}L_{\odot}$ ,  $10^{-3}L_{\odot}$ .

$M_p M_J$	$M_p$	$\alpha$	$R_{out}$ AU	$M_{disc}$		F(0.85mm)			F(1.3mm)			F(3mm)			$\overline{T}_b(0.85mm)$			$\overline{T}_b(1.3mm)$			$\overline{T}_b(3mm)$		
				$M_J$ $10^{-3}$	$M_J$ $10^{-5}$	$\mu Jy$ $10^{-3}$	$\mu Jy$ $10^{-4}$	$\mu Jy$ $10^{-5}$	$\mu Jy$ $10^{-3}$	$\mu Jy$ $10^{-4}$	$\mu Jy$ $10^{-5}$	$\mu Jy$ $10^{-3}$	$\mu Jy$ $10^{-4}$	$\mu Jy$ $10^{-5}$	K $10^{-3}$	K $10^{-4}$	K $10^{-5}$	K $10^{-3}$	K $10^{-4}$	K $10^{-5}$	K $10^{-3}$	K $10^{-4}$	K $10^{-5}$
$M_p = 1M_J$																							
1e-5	1e-1	0.12	8.7e-5	8.7e-5	4.3e1	4.2e1	4.2e1	1.3e1	1.3e1	1.3e1	1.2	1.2	1.2	223	220	219	161	159	159	77	76	76	
1e-5	1e-2	0.12	5.5e-4	5.5e-4	7.4e1	7.3e1	7.3e1	3.5e1	3.5e1	3.5e1	7.4	7.3	7.3	382	380	380	424	422	422	476	475	475	
1e-5	1e-3	0.12	3.5e-3	3.5e-3	7.4e1	7.3e1	7.3e1	3.5e1	3.5e1	3.5e1	8.1	8.0	8.0	382	380	380	424	422	422	521	520	520	
1e-5	1e-4	0.12	2.2e-2	2.2e-2	7.4e1	7.3e1	7.3e1	3.5e1	3.5e1	3.5e1	8.1	8.0	8.0	382	380	380	424	422	422	521	520	520	
1e-5	1e-1	0.46	6.1e-4	6.1e-4	1.1e2	1.0e2	1.0e2	3.3e1	3.0e1	3.0e1	2.8	2.6	2.5	37	34	33	25	23	23	11	10	10	
1e-5	1e-2	0.46	3.8e-3	3.8e-3	4.3e2	4.2e2	4.2e2	1.9e2	1.8e2	1.8e2	2.1e1	2.1e1	2.1e1	140	136	136	143	140	140	87	85	85	
1e-5	1e-3	0.46	2.4e-2	2.4e-2	4.3e2	4.2e2	4.2e2	2.0e2	2.0e2	2.0e2	4.6e1	4.6e1	4.6e1	140	136	136	154	152	151	188	187	186	
1e-5	1e-4	0.46	1.5e-1	1.5e-1	4.3e2	4.2e2	4.2e2	2.0e2	2.0e2	2.0e2	4.6e1	4.6e1	4.6e1	140	136	136	154	152	151	188	187	186	
1e-5	1e-1	1.85	3.6e-3	4.2e-3	2.9e2	2.4e2	2.3e2	8.1e1	6.9e1	6.5e1	6.7	5.8	5.4	5.79	4.95	4.62	3.85	3.30	3.08	1.70	1.46	1.36	
1e-5	1e-2	1.85	2.7e-2	2.7e-2	1.9e3	1.7e3	1.6e3	6.0e2	5.3e2	5.2e2	5.5e1	4.9e1	4.9e1	38	34	33	28	25	25	14	13	12	
1e-5	1e-3	1.85	1.7e-1	1.7e-1	2.6e3	2.4e3	2.4e3	1.2e3	1.1e3	1.1e3	2.7e2	2.6e2	2.6e2	53	49	48	57	54	54	68	67	66	
1e-5	1e-4	1.85	1.1	1.1	2.6e3	2.4e3	2.4e3	1.2e3	1.1e3	1.1e3	2.7e2	2.6e2	2.6e2	53	49	48	57	54	54	68	67	66	
1e-6	1e-1	0.12	2.1e-5	2.2e-5	6.5	5.5	5.2	1.9	1.6	1.5	1.5e-1	1.3e-1	1.2e-1	34	28	27	22	19	18	10	8	8	
1e-6	1e-2	0.12	1.4e-4	1.4e-4	3.8e1	3.5e1	3.5e1	1.3e1	1.2e1	1.2e1	1.2	1.1	1.1	199	183	182	155	143	142	79	74	73	
1e-6	1e-3	0.12	8.7e-4	8.7e-4	4.4e1	4.1e1	4.1e1	2.0e1	2.0e1	2.0e1	4.6	4.5	4.5	227	215	214	248	238	237	298	293	293	
1e-6	1e-4	0.12	5.5e-3	5.5e-3	4.4e1	4.1e1	4.1e1	2.0e1	2.0e1	2.0e1	4.6	4.5	4.5	227	215	214	248	238	237	298	293	293	
1e-6	1e-1	0.46	9.6e-5	1.5e-4	1.5e1	1.4e1	1.2e1	4.2	3.9	3.3	3.4e-1	3.2e-1	2.7e-1	4.88	4.46	3.81	3.21	2.94	2.51	1.39	1.27	1.09	
1e-6	1e-2	0.46	8.7e-4	9.6e-4	1.2e2	1.0e2	9.6e1	3.6e1	3.0e1	2.9e1	3.1	2.7	2.5	40	33	31	28	23	22	13	11	10	
1e-6	1e-3	0.46	6.1e-3	6.1e-3	2.8e2	2.4e2	2.4e2	1.3e2	1.1e2	1.1e2	2.0e1	1.9e1	1.8e1	91	79	77	97	87	85	83	75	74	
1e-6	1e-4	0.46	3.8e-2	3.8e-2	2.8e2	2.4e2	2.4e2	1.3e2	1.1e2	1.1e2	2.0e1	1.9e1	1.8e1	91	79	77	97	87	85	112	106	105	
1e-6	1e-1	1.85	4.0e-4	9.6e-4	3.2e1	3.1e1	2.8e1	9.0	8.6	8.0	7.3e-1	7.0e-1	6.5e-1	0.65	0.63	0.58	0.43	0.41	0.38	0.18	0.18	0.16	
1e-6	1e-2	1.85	3.9e-3	6.7e-3	2.9e2	2.7e2	2.7e2	8.4e1	7.8e1	6.8e1	7.0	6.5	5.7	5.95	5.52	4.78	3.99	3.70	3.22	1.78	1.65	1.44	
1e-6	1e-3	1.85	3.6e-2	4.2e-2	1.7e3	1.4e3	1.3e3	6.0e2	5.0e2	4.6e2	6.0e1	5.0e1	4.7e1	35	29	27	28	24	22	15	13	12	
1e-6	1e-4	1.85	2.7e-1	2.7e-1	2.0e3	1.5e3	1.4e3	8.8e2	6.8e2	6.4e2	1.8e2	1.5e2	1.5e2	40	30	28	42	32	31	45	38	37	
1e-7	1e-1	0.12	2.5e-6	5.5e-6	7.6e-1	7.1e-1	6.2e-1	2.1e-1	2.0e-1	1.7e-1	1.7e-2	1.6e-2	1.4e-2	3.93	3.70	3.20	2.57	2.42	2.09	1.11	1.05	0.91	
1e-7	1e-2	0.12	2.4e-5	3.5e-5	6.9	6.1	5.2	2.0	1.8	1.5	1.6e-1	1.5e-1	1.3e-1	35.77	31.76	26.98	24.06	21.39	18.26	10.64	9.47	8.11	
1e-7	1e-3	0.12	1.4e-4	2.2e-4	3.2e1	2.5e1	2.3e1	1.2e1	1.0e1	9.6	1.3	1.1	1.1	166	128	121	151	124	117	86.81	71.67	68.18	
1e-7	1e-4	0.12	1.4e-3	1.4e-3	3.2e1	2.5e1	2.3e1	1.4e1	1.1e1	1.1e1	2.9	2.6	2.5	166	128	121	172	139	134	190	168	165	
1e-7	1e-1	0.46	1.0e-5	2.9e-5	1.6	1.6	1.5	4.5e-1	4.4e-1	4.1e-1	3.6e-2	3.5e-2	3.4e-2	0.52	0.51	0.48	0.34	0.33	0.31	0.15	0.14	0.14	
1e-7	1e-2	0.46	9.6e-4	2.4e-4	1.5e1	1.5e1	1.3e1	4.3	4.1	3.7	3.6e-1	3.4e-1	3.1e-1	4.98	4.76	4.26	3.30	3.15	2.82	1.44	1.38	1.24	
1e-7	1e-3	0.46	9.6e-3	1.5e-3	1.2e2	1.1e2	8.9e1	3.6e1	3.3e1	2.8e1	3.3	3.0	2.5	37.93	34.79	28.77	27.46	25.24	21.06	13.25	12.07	10.23	
1e-7	1e-4	0.46	8.7e-3	9.6e-3	2.4e2	1.6e2	1.4e2	1.0e2	7.2e1	6.4e1	1.9e1	1.5e1	1.4e1	78.11	51.48	44.20	79.18	54.58	48.71	75.68	61.48	57.49	
1e-7	1e-1	1.85	4.0e-5	1.2e-4	3.3	3.3	3.2	9.2e-1	9.1e-1	8.9e-1	7.5e-2	7.4e-2	7.2e-2	0.07	0.07	0.06	0.04	0.04	0.02	0.02	0.02	0.02	
1e-7	1e-2	1.85	4.0e-4	1.1e-3	3.2e1	3.2e1	3.0e1	9.1	8.9	8.5	7.4e-1	7.3e-1	6.9e-1	0.66	0.64	0.61	0.43	0.42	0.40	0.19	0.18	0.18	
1e-7	1e-3	1.85	4.0e-3	9.6e-3	2.9e2	2.8e2	2.8e2	8.4e1	8.1e1	7.4e1	7.1	6.9	6.3	5.81	5.64	5.17	3.97	3.84	3.52	1.80	1.74	1.60	
1e-7	1e-4	1.85	3.9e-2	6.7e-2	1.6e3	1.1e3	8.6e2	5.6e2	4.6e2	3.8e2	5.7e1	5.4e1	4.6e1	33.32	23.00	17.39	26.39	21.69	18.24	14.50	13.60	11.62	
1e-8	1e-1	0.12	2.5e-7	7.7e-7	7.9e-2	7.7e-2	7.4e-2	2.2e-2	2.2e-2	2.1e-2	1.8e-3	1.8e-3	1.7e-3	0.41	0.40	0.39	0.27	0.26	0.25	0.12	0.11	0.11	
1e-8	1e-2	0.12	2.5e-6	7.2e-6	7.8e-1	7.5e-1	7.0e-1	2.2e-1	2.1e-1	2.0e-1	1.8e-2	1.7e-2	1.6e-2	4.03	3.89	3.63	2.64	2.54	2.37	1.14	1.10	1.03	
1e-8	1e-3	0.12	2.5e-5	5.5e-5	6.7	6.4	5.5	2.0	1.9	1.6	1.7e-1	1.6e-1	1.4e-1	35.02	33.39	28.68	24.15	22.97	19.76	11.03	10.40	8.99	
1e-8	1e-4	0.12	2.4e-4	3.5e-4	3.0e1	1.8e1	1.4e1	1.1e1	1.0e1	8.0	6.4	1.3	1.2	9.6e-1	154	94	72	137	97	78.37	83.52	74.90	62.33
1e-8	1e-1	0.46	1.0e-6	3.1e-6	1.6e-1	1.6e-1	1.6e-1	4.6e-2	4.5e-2	4.4e-2	3.7e-3	3.7e-3	3.6e-3	0.05	0.05	0.05	0.03	0.03	0.03	0.02	0.01	0.01	
1e-8	1e-2	0.46	1.0e-5	3.1e-5	1.6	1.6	1.5	4.5e-1	4.5e-1	4.3e-1	3.7e-2	3.6e-2	3.5e-2	0.53	0.52	0.50	0.34	0.34	0.33	0.15	0.15	0.14	
1e-8	1e-3	0.46	1.0e-4	2.9e-4	1.5e1	1.5e1	1.4e1	4.3	4.3	4.0	3.6e-1	3.5e-1	3.3e-1	4.93	4.83	4.59	3.30	3.23	3.06	1.47	1.43	1.35	
1e-8	1e-4	0.46	9.9e-4	2.4e-3	1.1e2	9.8e1	8.3e1	3.5e1	3.2e1	2.9e1	3.2	3.1	2.8	36.98	31.74	27.11	26.48	24.14	21.70	12.99	12.54	11.17	
1e-8	1e-1	1.85	4.0e-6	1.2e-5	3.3e-1	3.3e-1	3.3e-1	9.3e-2	9.3e-2	9.2e-2	7.6e-3	7.5e-3	7.5e-3	0.01	0.01	0.01	0.00	0.00	0.00	0.00	0.00	0.00	
1e-8	1e-2	1.85	4.0e-5	1.2e-4	3.3	3.3	3.2	9.3e-1	9.2e-1	9.1e-1	7.6e-2	7.5e-2	7.4e-2	0.07	0.07	0.07	0.04	0.04	0.04	0.02	0.02	0.02	
1e-8	1e-3	1.85	4.0e-4	1.2e-3	3.2e1	3.2e1	3.1e1	9.1	9.0	8.8	7.5e-1	7.4e-1	7.2e-1	0.65	0.65	0.63	0.43	0.43	0.42	0.19	0.19	0.18	
1e-8	1e-4	1.85	4.0e-3	1.1e-2	2.8e2	2.7e2	2.5e2	8.2e1	7.9e1	7.6e1	7.1	7.0	6.7	5.75	5.42	5.16	3.90	3.76	3.63	1.79	1.76	1.68	
$M_p = 10M_J$ , $R_{out}$ of 0.12, 0.46, 1.85 AU corresponds to CPDs around a $10 M_J$ planet at 2.3, 9.3, 37 AU from the central solar mass star.																							
1e-5	1e-1	0.12	3.5e-5	3.5e-5	1.6e1	1.6e1	1.6e1	4.7	4.6	4.6	4.0e-1	3.8e-1	3.8e-1	85	83	82	58	56	56	26	25	25	
1e-5	1e-2	0.12	2.2e-4	2.2e-4	7.4e1	7.3e1	7.3e1	3.0e1	3.0e1	3.0e1	3.3	3.3	3.3	382	380	380	370	367	367	216	214	214	
1e-5	1e-3	0.12	1.4e-3	1.4e-3	7.4e1	7.3e1	7.3e1	3.5e1	3.5e1	3.5e1	8.1	8.0	8.0	382	380	380	424	422	422	521	520	520	
1e-5	1e-4	0.12	8.7e-3	8.7e-3	7.4e1	7.3e1	7.3e1	3.5e1	3.5e1	3.5e1	8.1	8.0	8.0	382	380	380	424	422	422	521	520	520	

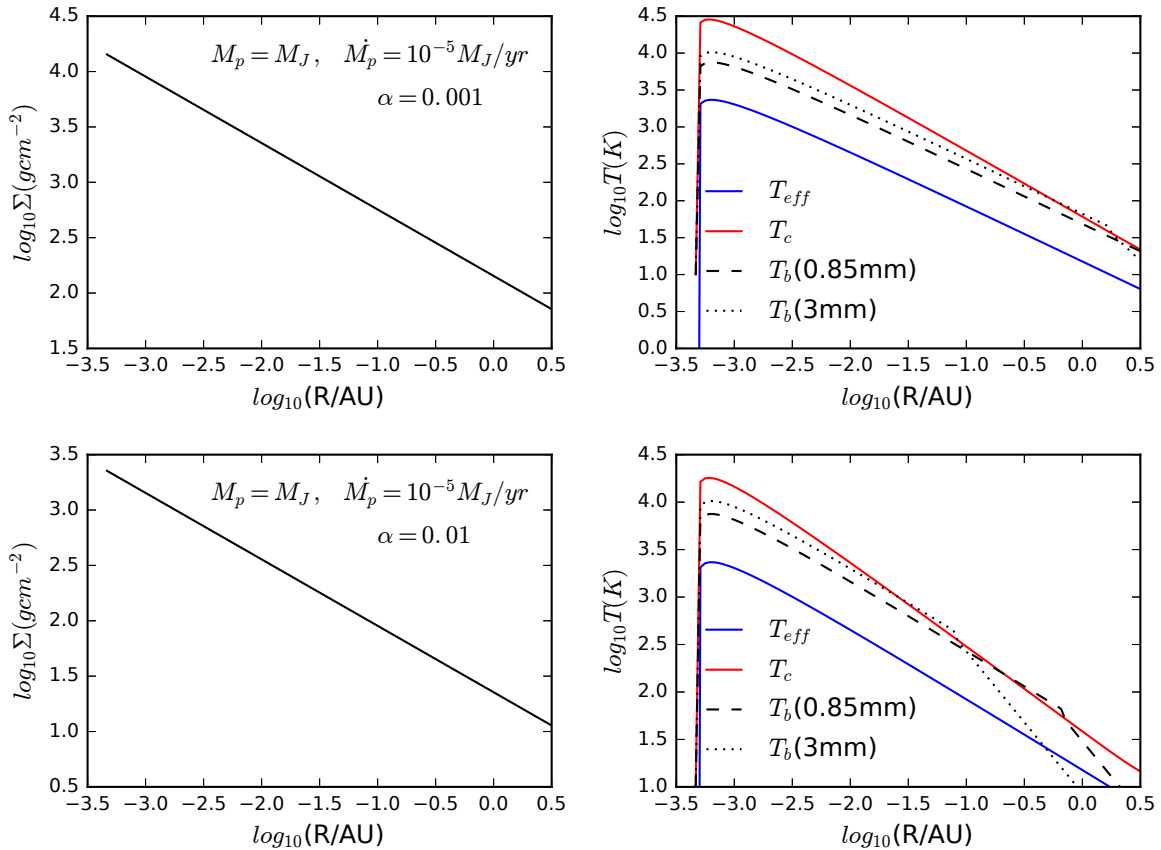


**Figure 1.** The disc surface density (left panels) and temperatures (right panels) for viscous heating dominated CPDs with  $\dot{M}_p = 10^{-5} M_J/\text{yr}$ ,  $M_p = 1M_J$ , and  $\alpha=0.001$  (upper panels) or  $\alpha=0.01$  (lower panels). Disc effective temperature, midplane temperature, effective brightness temperature at 0.85 mm and 3mm are shown in the right panels.

the flux is independent of the disc surface density and the integrated flux roughly scales as  $R_{out}^{1.27}$ . Thus, a CPD at 80 AU is almost 34 times brighter than the CPD at 5 AU as long as it is optically thick. On the other hand, when the disc becomes optically thin, the flux scales as  $R_{out}^{0.58}$ . Thus, a CPD at 80 AU will only be 5 times brighter than the CPD at 5 AU when the disc is optically thin.

Figure 3 shows the total flux at 0.85 mm (ALMA band 7) for CPDs with  $R_{out} = 0.48 \text{ AU}$ , or equivalently CPDs at  $a_p = 20 \text{ AU}$  with  $M_p = 1M_J$  and  $M_* = M_\odot$ . The flux is scaled by assuming that the systems are 140 pc away from us. The two most plausible  $\alpha$  values ( $\alpha=0.001$ , and 0.01 as in Zhu et al. 2016) are shown. The horizontal line is the  $5\sigma$  detection level ( $56 \mu\text{Jy}$ ) achieved by ALMA band 7 observation with 5 hours of integration on source <sup>3</sup>. As shown in the figure, the flux is independent of the  $\alpha$  value when the accretion rate is high ( $M_p \dot{M}_p = 10^{-5} M_J^2/\text{yr}$ ), since the discs are optically thick under such high accretion rates. When the accretion rate gets lower, the discs become optically thin at mm/cm and their brightness depends on their surface

density. The discs with lower  $\alpha$  values (triangles) are brighter since they have higher surface density. Overall, CPDs at 20 AU should be detectable with ALMA unless the disc’s accretion rate is very low  $M_p \dot{M}_p = 10^{-7} M_J^2/\text{yr}$  and  $\alpha$  is large ( $\alpha \geq 0.01$ ).

We summarize our results of Table 1 in Figure 4. From left to right,  $R_{out}$  is 0.12 AU, 0.46 AU, and 1.85 AU, or equivalent to a CPD around a Jupiter mass planet that is 5 AU, 20 AU, and 80 AU away from a solar mass star. Both Table 1 and Figure 4 clearly show that the disc’s radio emission decreases dramatically at longer wavelengths. In the optically thin limit with the above opacity law, the flux will decrease as  $\lambda^3$ . At VLA bands, the disc is normally 1-3 orders of magnitude fainter compared with the flux at ALMA bands. On the other hand, the RMS noise of VLA is less than a factor of 3 smaller than the RMS noise of ALMA <sup>4</sup>. Thus, ALMA will be much more sensitive to CPDs than VLA. On the other hand, ngVLA may be as sensitive as ALMA for detecting CPDs. The upper panels of Figure 4 show the flux at ALMA band 7 (red) and 6 (black), while the lower panels show the flux at ngVLA bands at 3 mm and 10 mm. The horizontal lines are the  $5\sigma$  detection levels achieved by 5 hours integration at each band. For ngVLA, we assume the 1-hour noise RMS is  $1.48 \mu\text{Jy}$  at 3 mm and  $0.39 \mu\text{Jy}$

<sup>3</sup> Using ESO ALMA sensitivity calculator for a source that transits overhead, the 1-hour RMS noise level of ALMA band 7 (345 GHz) is  $25 \mu\text{Jy}/\text{beam}$  and the 1-hour RMS noise level of ALMA band 6 (230 GHz) is  $16 \mu\text{Jy}/\text{beam}$ , assuming the maximum bandwidth (7.5 GHz per polarization) for 43 antennas in the “automatic” weather conditions.

<sup>4</sup> Using the VLA exposure calculator, we derive that the 1-hour RMS noise of the A array Q band observation is  $10 \mu\text{Jy}$ .

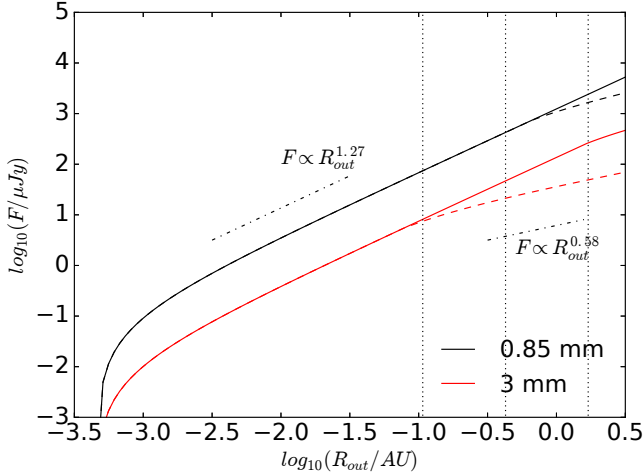


**Figure 2.** The integrated flux as a function of the disc outer radius  $R_{out}$ .  $\dot{M}_p$  is  $10^{-5} M_J/\text{yr}$  and  $M_p = 1 M_J$ . The disc is assumed to be viscous heating dominated, and thus the planet irradiation is not considered. The black and red curves show the flux at 0.85 mm and 3mm. The solid curves are for the case with  $\alpha = 0.001$  while the dashed curves are for the case with  $\alpha = 0.01$ . The vertical dotted lines label the three different disc sizes  $R_{out} = 0.12, 0.46,$  and  $1.85$  AU. When the disc becomes optically thin at a particular wavelength, the flux increases slower with  $R_{out}$ . The flux is calculated assuming the CPD is 140 pc away from us.

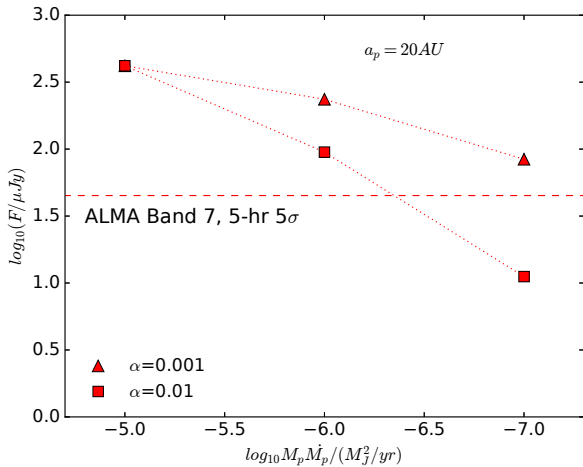


**Figure 3.** The flux at 0.85 mm (ALMA band 7) for viscous heating dominated CPDs with different accretion rates. The systems are assumed to be 140 pc away from us. Cases with two different  $\alpha$  values are shown. The planet mass is assumed to be  $1 M_J$  and the planet is 20 AU away from the central star ( $R_{out} = 0.46 \text{ AU}$ ). The horizontal line ( $56 \mu\text{Jy}$ ) is the  $5\sigma$  detection level at ALMA band 7 with 5 hours integration.

at 10 mm. Only discs with  $\alpha=0.001$  (triangles) and  $\alpha=0.01$  (squares) are shown in the figure. Figure 4 suggests that it is easier to detect CPDs at shorter radio wavelengths, and CPDs will also be bigger and brighter when they are further away from the star. With  $\alpha = 0.001$ ,  $M_p = 1 M_J$ , and  $M_* = M_\odot$ , 5 hours observation can safely detect CPDs that are more than 20 AU away from the central star and accret-

ing at  $\dot{M}_p \gtrsim 10^{-7} M_J/\text{yr}$ . If  $\alpha = 0.01$ , 5 hours observation can detect CPDs at 20 AU away from the star and accreting at  $\dot{M}_p \gtrsim 10^{-6} M_J/\text{yr}$ .

### 3.2 Irradiated Discs

When the irradiation from the planet dominates the viscous heating,  $T_c$  follows  $R^{-1/2}$  and  $\Sigma$  follows  $R^{-1}$  (Equations 3 and 7). For comparison,  $T_c$  and  $\Sigma$  of the viscously heated disc follow  $R^{-9/10}$  and  $R^{-3/5}$  (Equations 4 and 6). The disc structure for both viscous heating dominated and irradiation dominated discs is shown in the left panel of Figure 5. The disc surface density drops more sharply when the irradiation starts dominating the viscous heating. On the other hand, the right panel of Figure 5 shows that the effective brightness temperature and the mm/cm flux do not change much between the irradiated and viscous cases. This is because  $T_c \times \Sigma$  follows  $R^{-1.5}$  for both the viscously heated and irradiated discs, and  $T_c \times \Sigma$  is proportional to the effective brightness temperature when the disc is optically thin. This looks like a coincident, but it is the direct cause from the viscous accretion theory. Equation 5 suggests that

$$T_c \Sigma = \frac{\dot{M} \Omega \mu}{3\pi \alpha \Re} \quad (10)$$

when  $R \gg R_{in}$ . Thus, whatever the heating mechanism is,  $T_c \times \Sigma$  is unchanged and directly determined by  $\dot{M}$ . As shown in Table 2, the flux difference between cases with  $L_p = 10^{-3} L_\odot$  and cases with  $L_p = 10^{-5} L_\odot$  is normally  $< 10\%$ . In rare cases, the difference can go up to 30%.

## 4 DISCUSSION

### 4.1 CPD Models With Different Assumptions

Our calculations suggest that CPDs should be detectable by ALMA (note the caveat in §4.6). Here we will explore how the calculated flux will change if we relax some of our assumptions.

Our disc model in §2 (Equation 1) assumes a zero torque inner boundary, which means that the disc rotates at the local Keplerian speed at the inner boundary. In reality, the Keplerian rotating disc joins the slowly rotating planet through a boundary layer or magnetosphere channels. Unless the planet has strong magnetic fields (more discussion in Zhu 2015), a boundary layer will form between the disc and the planet, where half of the accretion energy ( $L_{acc} = GM_p \dot{M}_p / R_p$ ) is released. This boundary layer could irradiate and heat up the CPD. To include this effect, we set  $L_{irr} = 0.5 L_{acc}$  in Equations 1-7. The resulting mm/cm flux from such discs are shown on the right side of each  $T_b$  and flux column in Table 1. We can see that the irradiation has little effect on the mm emission. Only when the disc accretion rate is low and  $\alpha$  is large (in other words, the surface density is low), the irradiation can increase the total flux by 20%.

If the CPD is close to the star, the irradiation from the star and the circumstellar disc can be significantly stronger. At 5 AU, the circumstellar disc has a temperature of  $\sim 100$  K. We thus calculate the radio emission from CPDs with  $T_{ISM} = 100$  K which mimics the irradiation from the star and the circumstellar disc. The fluxes are shown as the plus signs in Figure 6. As expected from the argument in §3.2,

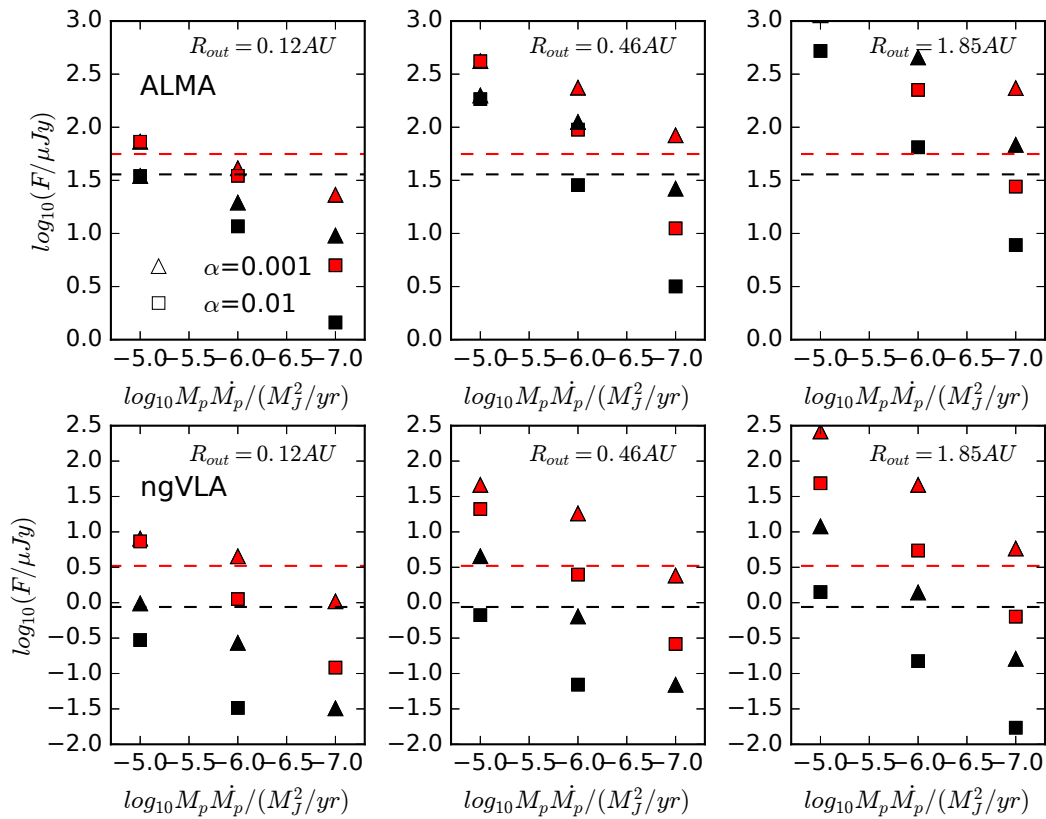


**Figure 4.** The flux for viscous heating dominated CPDs with different accretion rates. The upper panels show fluxes at 0.85 mm and 1.3 mm (red and black symbols, respectively). The red and black dashed lines indicate the  $5\sigma$  level achieved by ALMA respectively at 0.85 mm and 1.3 mm with 5 hours of integration on source. The lower panels show fluxes at 3 mm and 10 mm (red and black symbols, respectively). The red and black dashed lines ( $3.31 \mu Jy$  and  $0.87 \mu Jy$ ) indicate the  $5\sigma$  level achieved by 5 hours ngVLA observation with the assumed RMS noise level at these two bands (1-hour RMS noise of  $1.48 \mu Jy$  at 3 mm and  $0.39 \mu Jy$  at 10 mm). From left to right panels,  $R_{out}$  are 0.12 AU, 0.46 AU, and 1.85 AU, which correspond to  $a_p$  of 5 AU, 20 AU, and 80 AU for a Jupiter mass planet around a solar mass star. Triangles are the cases with  $\alpha=0.001$  while squares are the cases with  $\alpha=0.01$ .

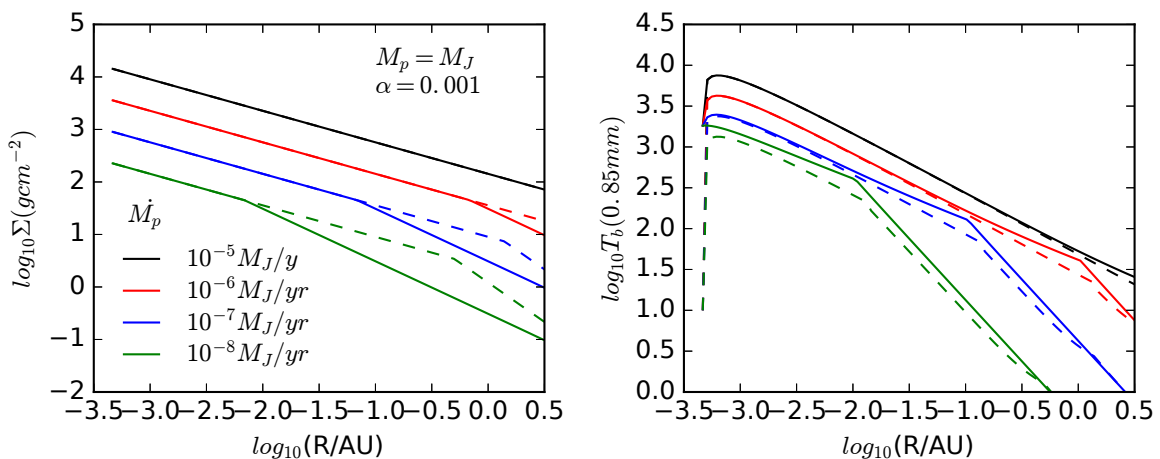


**Figure 5.** The radial profiles of the disc surface density and effective brightness temperature for discs without irradiation (dashed curves) and with irradiation (solid curves). For the irradiated cases, the central planet is assumed to have the luminosity of  $0.001 L_{\odot}$ .

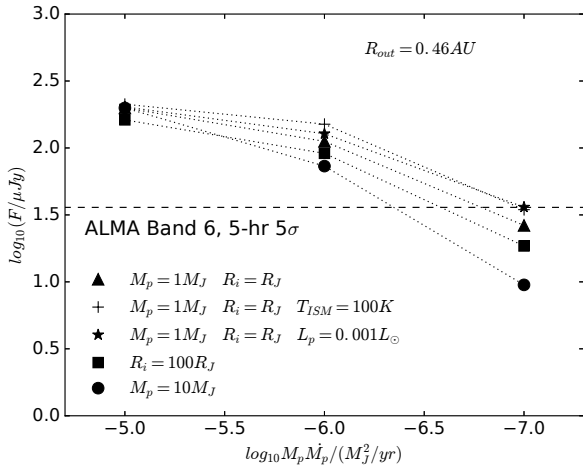


**Figure 6.** The flux at 1.3 mm (ALMA band 6) for CPDs with different accretion rates. All these cases have  $M_p \dot{M}_p = 10^{-5} M_J^2/\text{yr}$ ,  $\alpha=0.001$ , and  $R_{out} = 0.46$  AU. Cases with different background irradiation ( $T_{ISM}$ ), planet irradiation, planet masses ( $M_p$ ), and inner radii ( $R_i$ ) are shown. The horizontal line ( $36 \mu\text{Jy}$ ) is the  $5\sigma$  detection level at ALMA band 6 with 5 hours integration.

such strong irradiation has little effect on the disc’s radio emission.

The irradiation onto the disc can also be strong if the planet is bright by itself (e.g. it has a “hot start”). But as shown in Table 2 and §3.2, irradiation does not change the mm emission significantly because the flux in the optically thin limit only depends on the accretion rate and is independent of the heating mechanism. The mm emission from the CPDs irradiated by a  $L = 0.001L_\odot$  planet is shown in Figure 6 as the star signs and they are quite similar to the non-irradiated case.

Then, we explore how the mm emission changes if we vary  $R_{in}$  in the model. The size of a young Jupiter mass planet could be larger than  $R_J$  if it starts with a high internal energy (Marley et al. 2007). A young planet may also have strong magnetic fields, truncating the CPD far away from the planet. For the emission at near-IR and mid-IR, Zhu (2015) has shown that the IR flux is very sensitive to  $R_{in}$  since most near-IR/mid-IR emission comes from the inner disc. On the other hand, we expect CPD’s mm/cm flux is sensitive to  $R_{out}$  instead of  $R_{in}$ , since most mm/cm emission comes from the outer disc. We demonstrate this point in Figure 6. Even with  $R_i=100R_J$ , the mm/cm flux is almost unchanged.

Our models assume that  $R_{out}$  is 1/3 of the Hill radius, which is supported by many theoretical studies (Quillen & Trilling 1998; Martin & Lubow 2011). However, in case  $R_{out}$  is smaller than this value by a factor of 2, the total flux will only decrease by a factor of 2.4 if the disc is optically thick or by a factor of 1.5 if the disc is optically thin (the scaling law is given in Figure 2).

Finally, we study how the mm/cm flux changes with different  $M_p$ . Since the disc’s effective temperature only depends on  $M_p \dot{M}_p$ , at a given  $M_p \dot{M}_p$ , the flux will be independent of  $M_p$  when the disc is optically thick at mm/cm. On the other hand,  $T_c \Sigma$  depends on  $\dot{M}_p M_p^{1/2}$  (Equation 10). Thus, when the disc is optically thin, mm/cm flux should roughly scale with  $M_p^{-1/2}$  at a given  $M_p \dot{M}_p$ . This has been

shown in Figure 6. With  $M_p \dot{M}_p = 10^{-5} M_J^2/\text{yr}$  fixed, the flux from the CPD around a  $10M_J$  planet is almost the same as the flux from the CPD around a  $1 M_J$  planet since the disk is optically thick. But with  $M_p \dot{M}_p = 10^{-7} M_J^2/\text{yr}$ , the flux from the  $M_p = 10M_J$  case is a factor of  $\sim 3$  smaller than the  $M_p = 1M_J$  case.

Overall, our calculated mm/cm flux is robust and it is not affected by the boundary layer, the irradiation, the inner disc radius, and only mildly affected by  $M_p$ .

## 4.2 Radio Flux From Minimum Mass Sub-nebula Model

Although we have little observational constraints on CPDs around young planets, we can use satellites around Jovian planets in our solar system to study CPDs that were in our solar system. Several CPD models have been constructed to understand satellite formation in our solar system 5 billion years ago. In one model, by spreading the mass of Galilean satellites into a mini disc around Jupiter, the “minimum mass sub-nebula” disc was constructed (Lunine & Stevenson 1982; Mosqueira & Estrada 2003). Such model has a high gas surface density of  $\text{few} \times 10^5 \text{ g cm}^{-2}$ . The disc surface density and temperature in Mosqueira & Estrada (2003) are plotted in the left and middle panel of Figure 7. In this model, the disc is assumed to have the same temperature along the vertical direction. We calculate the disc effective brightness temperature and integrate the total mm/cm emission from the disc (the right panel of Figure 7). Surprisingly, such a disc at 5 AU (so  $R_{out} \sim 0.12$  AU) is even detectable by ALMA. Thus, if the “minimum mass sub-nebula” disc once existed around our Jupiter, we will be able to detect such a disc in a young solar system analog 140 pc away. In reality, the circumstellar material may confuse the detection even with ALMA’s highest resolution unless a deep gap has been carved out (more discussion in §4.5). On the other hand, the other satellite formation model, so-called “gas-starved” disc model (Canup & Ward 2002), has a much lower surface density. The “gas-starved” disc model is basically an  $\alpha$  disc model with  $\dot{M}_p \sim 2 \times 10^{-7} M_J/\text{yr}$ , so its mm/cm emission can be found from our main set of models. We will be able to detect such CPDs if they are 20 AU away from the central star with  $\alpha < 0.01$ .

## 4.3 Radio Emission from CPD Jets and Winds

Most astrophysical accretion discs, from AGNs to protostars, produce jets and winds that are observable at both radio and optical wavelengths. Thus, accreting CPDs could also produce jets and winds. MHD simulations by Gressel et al. (2013) have indeed suggested that disc winds can be launched in CPDs. To estimate the centimetre free-free emission of jets launched in CPDs, we extrapolate the relationship for protostellar jets given in Anglada et al. (2015),

$$\frac{F_\nu d^2}{mJy \text{ kpc}^2} = 0.008 \left( \frac{L_{bol}}{L_\odot} \right)^{0.6} \quad (11)$$

to the planetary mass regime. With  $L_{bol} = 1.57 \times 10^{-3} L_\odot$  in our  $M_p \dot{M}_p = 10^{-5} M_J^2/\text{yr}$  model, we can estimate that  $F_\nu$  from the jet is  $8.48 \mu\text{Jy}$  at  $d=140$  pc. The flux of  $8.48 \mu\text{Jy}$  is undetectable by ALMA, but it can be detected by ngVLA. Thus, when we have CPD detections with ngVLA

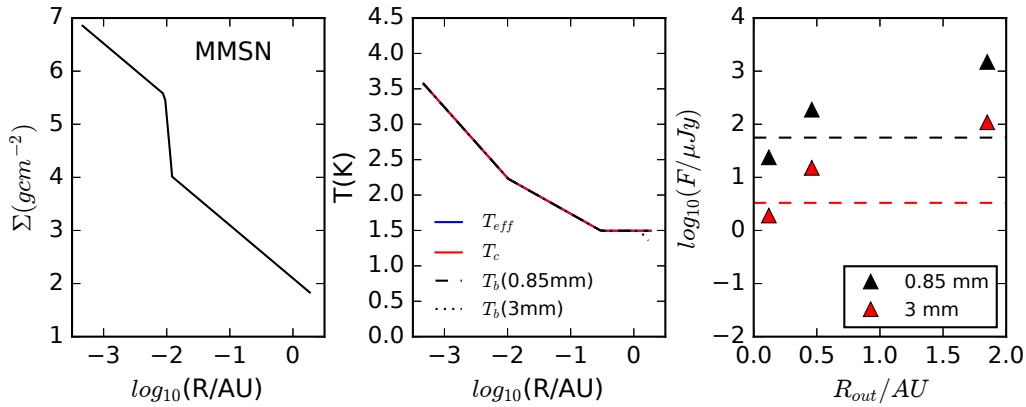


**Figure 7.** The minimum mass sub-nebula model and its mm/cm emission. The disc surface density and temperature (Mosqueira & Estrada 2003) are shown in the left and middle panel. The middle panel also shows the brightness temperature at 0.85 mm and 3 mm. Since the disc has a uniform temperature vertically and the disc is optically thick, the effective brightness temperature equals the disc midplane temperature. The integrated mm/cm emission for discs with different  $R_{out}$  are shown in the right panel. The horizontal lines are the 5-hr  $5\sigma$  detection levels for ALMA and ngVLA.

in future, we may need to separate the flux from the disc and the flux from the jet using the radio spectral index, similar to the practice we are carrying out in the circumstellar discs (e.g. Carrasco-González et al. 2016).

We caution that such extrapolation using Equation 11 is extremely crude without any physical argument to support. The extrapolated flux can be off by more than one order of magnitude. Nevertheless, this provides a rough estimate of the possible radio emission from the disc.

#### 4.4 Constraining CPD properties

If there is ALMA detection of discs around planetary mass objects, we can use our disc models to constrain CPD properties. We take the recent ALMA detection of the disc around OTS44 (a  $12M_J$  object) as an example (Bayo et al. 2017). OTS44 accretes at  $8 \times 10^{-12} M_\odot/\text{yr}$ . Thus,  $\dot{M} \sim 10^{-7} M_J^2/\text{yr}$ . The source is detected at  $\sim 100 \mu\text{Jy}$  at ALMA Band 6. Since the disc is unresolved by ALMA with the beam of  $0.16''$ , the disc size is smaller than 13 AU with the distance of 160 pc. All our models satisfy this size constraint. By using Table 2 and under the  $M_p = 10M_J$ ,  $\dot{M} \sim 10^{-7} M_J^2/\text{yr}$ ,  $L = 0.001L_\odot$  category, we can find that the disc mass is around  $0.01 M_J$  and  $R_{out} \sim 1\text{AU}$  if  $\alpha = 10^{-4}$ . If  $\alpha = 10^{-3}$ , the CPD with  $R_{out} = 1.85\text{AU}$  has a flux of  $28 \mu\text{Jy}$  and a mass of  $1.3 \times 10^{-3} M_J$ . As discussed in §3.1, the flux scales as  $R_{out}^{0.58}$  when the disc is optically thin, and the mass scale as  $R_{out}^1$  for strongly irradiated discs. Thus, to emit  $100 \mu\text{Jy}$ , the disc has a outer radius of 17 AU and also a mass of  $0.01M_J$  with  $\alpha = 10^{-3}$ .

The disc mass and mm emission for all our models are given in the left panel of Figure 8. We can see that the 5 hours ALMA Band 7 observation can probe CPDs having  $10^{-4} M_J$  of gas, which is equivalent to 0.026 lunar mass of dust assuming the dust-to-gas mass ratio of 1/100. There is a loose correlation between the disc mass and the mm emission. Thus, by using such correlation, we can estimate the disc mass from its mm emission. From Table 2, we see that the flux at ALMA Band 7 is roughly 3 times larger than the flux at Band 6. Thus, for OTS 44, the flux at ALMA Band

7 should be around  $300 \mu\text{Jy}$ . Using Figure 8, the estimated disc mass for OTS 44 is again  $0.01M_J$ .

On the other hand, OTS 44 is a free floating planetary mass object whose outer disc radius is unconstrained. For a planetary mass object orbiting around a central star, its outer radius is limited to 1/3 of its Hill radius. Thus, knowing the planet’s position with respect to the central star,  $R_{out}$  can also be estimated with some assumptions about the planet and the stellar mass. Then, both the CPD’s radio flux and  $R_{out}$  are known. We plot the mm emission and  $R_{out}$  for all our models in the right panel of Figure 8.

We can apply this figure to the recent ALMA tentative detection of the point source within HD 142527 (Boehler et al. 2017). HD 142527 system is  $\sim 156\text{pc}$  away from us. The point source candidate is at 50 AU from the central star and has the flux of  $0.80\text{mJy}$  at  $0.88\text{mm}$ . The right panel of Figure 8 suggests that the upper flux limit from the CPDs at  $\sim 50\text{AU}$  is  $\sim 2\text{mJy}$ . Thus, the detected flux is consistent with the emission from the CPD. Since the measured flux is close to the upper limit of all the models, the CPD candidate is almost optically thick at mm and the  $M_p \dot{M}_p$  should be  $\gtrsim 10^{-7} M_J^2/\text{yr}$  based on the figure. If the inner radius of the CPD is  $1 R_J$ , the CPD should be brighter than 17.2 magnitude at the mid-IR M band (Zhu 2015), which can be studied by JWST in future.

We can also use the right panel of Figure 8 to constrain the non-detection of discs around GSC 0614-210 b (Bowler et al. 2015), DH Tau b (Wolff et al. 2017) and GQ Lup B (MacGregor et al. 2017; Wu et al. 2017) by ALMA. The accretion rates of these discs have been measured with various techniques. DH Tau b has an accretion rate of  $3.2 \times 10^{-12} M_\odot/\text{yr}$  (Zhou et al. 2014), GQ Lup B has an accretion rate of  $10^{-12}$  to  $10^{-11} M_\odot/\text{yr}$  (Wu et al. 2017) (but see Zhou et al. 2014 which derive an accretion rate of  $10^{-9.3} M_\odot/\text{yr}$ ), and GSC 0614-210 b has an accretion rate of  $10^{-10.8} M_\odot/\text{yr}$  (Zhou et al. 2014). Thus,  $\dot{M}$  in these discs are  $\sim 10^{-8} - 10^{-7} M_J^2/\text{yr}$ . Assuming these discs fill 1/3 of their Hill radius, the non-detection may suggest that  $\alpha \gtrsim 0.001$  in these discs.

HD 169142b is another CPD candidate 20 AU away

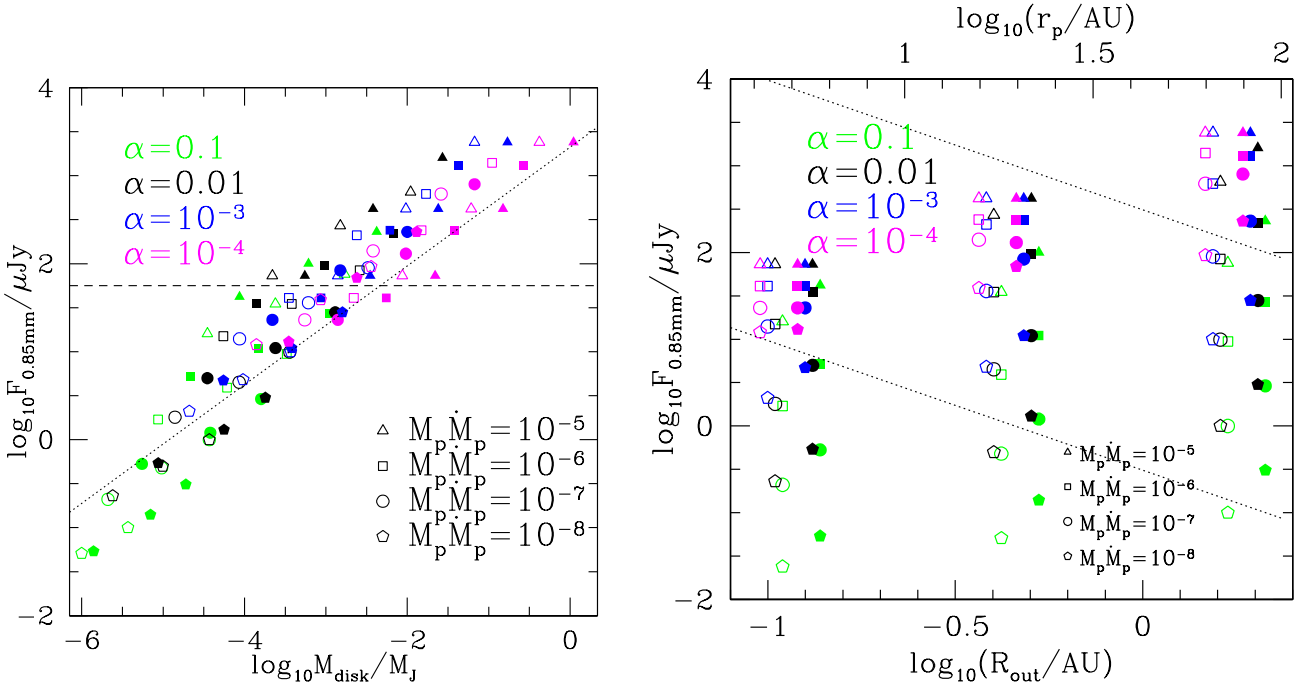


**Figure 8.** Left: The disc mass and submm emission (at 0.85 mm) for our models. Right: The disc outer radius and submm emission (at 0.85 mm) for our models. The filled points are discs with  $M_p = 1M_J$  (from Table 1 without boundary irradiation) while the open points are discs with  $M_p = 10M_J$  (from Table 2 with little irradiation,  $L_p = 10^{-5}L_\odot$ ). In the right panel, the distance of the planet from the central star is plotted on the top axis (assuming a Jupiter mass planet around a solar mass star) and the three  $R_{out}$  (0.12, 0.46, 1.85 AU) are slightly shifted horizontally to show overlapping points. The horizontal line in the left panel is the 5-hr  $5\sigma$  detection level for ALMA Band 7. The two dotted lines in the right panel represent the flux from the fiducial circumstellar disc (Equation 13) and the flux which is a factor of 1000 smaller than the fiducial case, assuming the ALMA Band 7 observation with the  $0.03''$  resolution.

from the central  $1.65 M_\odot$  star. If its L band emission comes from the accreting CPD (Reggiani et al. 2014), Zhu (2015) estimate that  $M_p \dot{M}_p$  is  $10^{-5} M_J^2/\text{yr}$ . Then Table 1 suggests that the disc should be around  $400 \mu\text{Jy}$  at ALMA Band 7, which is consistent with the estimate from numerical simulations in Zhu et al. (2016). Finally, we caution that we have assumed perfect coupling between dust and gas so far. If we relax this assumption, the discs without radio detections may still have a lot of gas despite very little dust, and HD 169142b may be faint at radio bands (more discussion in §4.6).

#### 4.5 The Resolution Requirement

In most above cases, the planet/brown dwarf is not embedded in the circumstellar disc so there is little confusion between the tiny disc around the brown dwarf/planet and the circumstellar disc around the central star. In reality, we want to discover CPDs within circumstellar discs or gaps of circumstellar discs. Then, we need to not only detect CPDs but also have enough spatial resolution to separate them from circumstellar discs. The emission from the background circumstellar disc or cavity/gap can be simply estimated assuming the disc is optically thin, which is normally a good approximation for the circumstellar disc region beyond 10 AU. Suppose the circumstellar disc has a surface density and temperature structure of  $\Sigma(r)$  and  $T(r)$ , the effective brightness temperature will be  $t_b(r) = T(r) \times \kappa_{mm} \times \Sigma(r)$ . If we choose a fiducial model with  $\Sigma(r) = 1.78 (r/100 \text{ AU})^{-1} \text{ g cm}^{-2}$  and  $T(r) = 22.1 (r/100 \text{ AU})^{-1/2} \text{ K}$ , which is a  $\alpha = 0.01$  disc around a solar mass star accreting at  $10^{-8} M_\odot \text{ yr}^{-1}$  and

roughly consistent with the protoplanetary discs in Ophiuchus (Andrews et al. 2009), we have

$$t_b(\lambda) = 1.34 \times \frac{\Sigma(r)}{1.78 \text{ g cm}^{-2}} \frac{T}{22.1 \text{ K}} \frac{0.87 \text{ mm}}{\lambda}. \quad (12)$$

Then, assuming the mm beam size is  $\theta$  and the source is 140 pc away, the radio flux will be

$$F(\lambda) = 87 \mu\text{Jy} \times \frac{\Sigma(r)}{1.78 \text{ g cm}^{-2}} \frac{T}{22.1 \text{ K}} \frac{0.87 \text{ mm}}{\lambda} \left( \frac{\theta}{0.03''} \right)^2. \quad (13)$$

With  $\Sigma(r) = 1.78 (r/100 \text{ AU})^{-1} \text{ g cm}^{-2}$  and  $T(r) = 22.1 (r/100 \text{ AU})^{-1/2} \text{ K}$ ,  $F(\lambda)$  follows  $r^{-1.5}$  and it is plotted in the right panel of Figure 8 assuming the  $0.03''$  resolution. Clearly with such high disc surface density, it is difficult to detect any CPD within 20 AU with  $0.03''$  resolution. To detect CPDs at 20 AU, the radio flux from the circumstellar disc within the telescope beam needs to be suppressed by at least 2-3 orders of magnitude. Such suppression can be physical due to the decrease of the surface density from the gap opening process, or can be observational such as using a smaller telescope beam. However, there is a limit of using a smaller beam. When the CPD starts to be spatially resolved, decreasing the beam size won't increase the contrast between the CPD and the circumstellar discs. For the CPD at 20 AU away from the central star,  $R_{out}$  is 0.46 AU so that this limiting spatial resolution is  $0.46 \text{ AU}/140 \text{ pc} = 0.0033''$ . We will achieve the maximum contrast between the CPD and the background circumstellar disc at this resolution. This is where ngVLA has more advantage than ALMA

with similar sensitivity level but much higher angular resolution.

Another advantage of using a high spatial resolution is that we can separate the gap region from the smooth circumstellar disc. A giant planet at  $r_p$  can induce a gap which can extend from  $0.5 r_p$  to  $2 r_p$ . If we can spatially resolve the gap, we can gain the maximum contrast between the gap and the CPD. We can also gain a higher contrast if the CPD is at the outer disc where the circumstellar disc has a lower surface density and a lower temperature, as shown by the dotted line in the right panel of Figure 8). Thus, to detect CPDs, we should observe discs with large gaps/cavities using the highest resolution possible.

#### 4.6 The drift of mm/cm dust particles

So far we have assumed that dust and gas are perfectly coupled. In reality, dust particles feel the aerodynamic drag force from the gas and drift radially in discs. The aerodynamic drag force depends on particle size and is normally parameterized using the dimensionless dust stopping time ( $T_s$ ). The radial drift speed is

$$v_{R,d} = \frac{T_s^{-1} v_{R,g} - \eta v_K}{T_s + T_s^{-1}}, \quad (14)$$

where  $v_{R,g}$  is the gas radial velocity,  $v_K$  is the midplane Keplerian velocity, and  $\eta = -(R\Omega_K^2 \rho_g)^{-1} \partial P_g / \partial R$  is the ratio between the gas pressure gradient and the stellar gravity in the radial direction (Weidenschilling 1977; Takeuchi & Lin 2002).

When the particle size is smaller than the mean free path of a molecule (which is the case for the problem studied here), the drag force is in the Epstein regime and  $T_s$  can be written as (e.g. Espaillat et al. 2014)

$$T_s = 1.55 \times 10^{-3} \frac{\rho_p}{1 \text{ g cm}^{-3}} \frac{s}{1 \text{ mm}} \frac{100 \text{ g cm}^{-2}}{\Sigma_g}, \quad (15)$$

where  $\rho_p$  is the dust particle density,  $s$  is the dust size, and  $\Sigma_g$  is the disc gas surface density.

With Equations 14 and 15, we can calculate the dust drift timescale

$$\tau_{drift} = \frac{R}{v_{R,d}} = \frac{T_s + T_s^{-1}}{2\pi \frac{\partial \ln P}{\partial \ln R} \left(\frac{H}{R}\right)^2} T_{orb}, \quad (16)$$

where  $T_{orb} = 2\pi/v_K$ . For irradiation dominated discs, we have  $\Sigma = \Sigma_0 (R/AU)^{-1}$  and  $T = T_0 (R/AU)^{-0.5}$ . For the particular case where  $M_p = 1M_J$ ,  $\dot{M}_p = 10^{-8} M_J/\text{yr}$ , and  $\alpha = 0.001$  (as in Figure 5), we have  $\Sigma_0 = 0.2 \text{ g cm}^{-2}$  and  $T_0 = 40 \text{ K}$ . Putting these values into Equation 16 and assuming  $T_s < 1$ , we derive the particle drift timescale

$$\tau_{drift} = 47.8 \frac{1 \text{ mm}}{s} \frac{\Sigma_0}{0.2 \text{ g cm}^{-2}} \frac{40 \text{ K}}{T_0} \left(\frac{M_p}{10 M_J}\right)^{1/2} \text{ yrs}, \quad (17)$$

which is extremely short. For a comparison, the gas accretion timescale is

$$\tau_{gas} = \frac{R^2}{\nu} = 10^5 \left(\frac{M_p}{10 M_J}\right)^{1/2} \frac{R}{AU} \frac{0.001}{\alpha} \frac{40 \text{ K}}{T_0} \text{ yrs}. \quad (18)$$

The drift timescale of mm particles in CPDs is 3 orders of magnitude smaller than the drift timescale of mm particles in circumstellar disks. For the circumstellar disc around a solar mass star, the central object mass is  $1000 M_J$ ,  $T_0$  is  $\sim 200 \text{ K}$ ,  $\Sigma_0$  is  $\sim 1000 \text{ g cm}^{-2}$  if  $\alpha = 0.001$ . Thus,  $\tau_{drift}$  is

$\sim 5 \times 10^5$  yrs for 1 mm dust particles. The drift timescale for the disc around a solar mass star is shown in the left panel of Figure 9. As the disc's surface density decreases and the mass of the central object drops,  $\tau_{drift}$  decreases significantly. For the  $10 M_J$  planet accreting at a low rate (shown in the right panel of Figure 9), the drift timescale for 1 mm particles is only 1000 years. This fast radial drift is consistent with the lack of mm emission from GSC 0614-210 b (Bowler et al. 2015), DH Tau b (Wolff et al. 2017) and GQ Lup B (MacGregor et al. 2017; Wu et al. 2017). It also suggests that there may still be a lot of gas in these discs, which can be probed by future ALMA molecular line observations.

Figure 10 shows the drift timescale for discs around a Jupiter mass planet. The 1 mm particles will drift to the central star within 1000 years even in discs accreting at  $10^{-9} M_\odot/\text{yr}$ . The drift timescale is  $< 100$  years when the disc accretes at  $10^{-11} M_\odot/\text{yr}$ . The upper panels show the irradiation dominated cases while the bottom panels show the viscous heating dominated cases. Clearly, independent of the heating mechanism, the drift timescale for mm particles is very short <sup>5</sup>.

The meter barrier in protoplanetary discs becomes the millimetre barrier in circumplanetary discs.

Thus, it is unlikely that we will detect mm/cm signals from discs around planetary mass objects unless:

1) There is a significant population of micron sized dust. At mm/cm wavelengths, the opacity of micron-sized dust is only several times smaller than that of mm-sized dust (D'Alessio et al. 2001). Thus, if all the dust in the CPD is in the micron-sized range, the CPD can still have detectable radio emission, although the flux will be weaker than our current estimate.

2) Or the disc has a high surface density so that the mm-sized dust has a smaller stopping time and the drift timescale is long. This means that the disc either accretes at a high rate or the  $\alpha$  is small.

3) Or dust is continuously being replenished into the disc. The replenishment could come from the accretion streams from the circumstellar disc, or infalling envelope, or dust fragmentation due to collisions between bigger dust particles<sup>6</sup>. On the other hand, the dust replenishing rate needs to be very high to compensate the fast radial drift. For example, if the radial drift timescale is  $10^2$  years while the gas accretion timescale is  $10^5$  years, the dust-to-gas mass ratio will be 1000 times smaller than the ISM value (0.01) even with the continuous replenishment of dust and gas.

4) Or there are structures in the gaseous CPD (e.g. pressure traps) which can slow down or even trap dust particles in the disc. In the CPD simulations by Zhu et al. (2016), rings and vortices have indeed been observed (e.g. Figure 3, 4 in that paper) due to the shock driven accretion. Although these features are transient, they may slow down particle radial drift.

Another possibility for the existence of dust is that

<sup>5</sup> When particles settle to the disc midplane or have significant pile up, the feedback from dust to gas becomes important. Then streaming instability (Youdin & Goodman 2005) will operate to regulate the dust to gas mass ratio, and dust will still drift fast radially (slower by a factor of 2 than the speed without including the feedback (Bai & Stone 2010)).

<sup>6</sup> The real situation can be a lot more complicated since dust particles may be trapped at the gap edge induced by the planet and won't be flow into the circumplanetary disc.

CPDs are in the debris disc stage so that there is little gas in the disc (dust to gas mass ratio  $\gtrsim 1$  and dust drift is slow). Since we are interested in CPDs that are actively accreting, this is beyond the scope of this paper.

Overall, it is more likely to detect discs around planetary mass objects if the discs are accreting at a relatively high rate (surface density is higher so that the dust drift timescale is longer) and being fed continuously (e.g. through circumstellar discs, infalling envelope, etc.). It is less likely to find discs around isolated planetary mass objects that are accreting at a low rate.

On the other hand, OTS44 is isolated and does not have a high accretion rate either. The mm particles should have already drifted to the central planetary mass object (the right panel of Figure 9). Based on the drift timescale argument, we suggest that the ALMA detection by Bayo et al. (2017) indicates that most dust may be at the micron-sized range, or the disk has sub-structures, or the gas surface density is very high so that the dust to gas mass ratio is significantly lower than 1/100. The latter scenario can be tested if its gas mass can be constrained from ALMA molecular line observations.

Another interesting source is FW Tau b (Kraus et al. 2014) which is a  $\sim 10 M_J$  companion 330 AU away from the central 0.2-0.3  $M_\odot$  binary. ALMA has detected a strong emission ( $\sim 1.78$  mJy) at 1.3 mm (Kraus et al. 2015), implying 1-2 earth mass of dust in the disc. This amount of dust mass implies 1  $M_J$  mass of gas (10% of the central object mass) in the disc with the assumption that the dust-to-gas mass ratio is 1/100. Considering the gravitational instability will limit the gas mass, it is unlikely that the dust-to-gas mass ratio can be significantly lower than 1/100 in this disc. We suggest that most of the radio emission may come from micron-sized dust in this disc, or there are structures in the disc to slow down the particle radial drift.

## 5 CONCLUSION

We have constructed simple  $\alpha$  disc models to study radio emission from circumplanetary discs (CPDs). A large disc parameter with  $M_p M_p$  from  $10^{-8} M_J^2/yr$  to  $10^{-5} M_J^2/yr$ ,  $\alpha$  from  $10^{-4}$  to  $10^{-1}$ , and  $R_{out}$  from 0.1 to 1.85 AU has been explored.

We find that radio observations are more sensitive to CPDs at shorter wavelengths (e.g. ALMA Band 7 and above). The radio emission by viscous discs is almost independent of the inner disc radius and the irradiation by the star or the planet. If the system is 140 pc away from us, deep observations at ALMA Band 7 could detect CPDs around a Jupiter mass planet at 20 AU from the host star, when the disc accretes at a rate of  $\gtrsim 10^{-10} M_\odot/yr$  with  $\alpha \lesssim 0.001$  or at a rate of  $\gtrsim 10^{-9} M_\odot/yr$  with  $\alpha \lesssim 0.01$ . When the CPDs are closer or further away from the star, we can scale our calculated flux accordingly: the flux scales as  $R_{out}^{1.27}$  when the CPD is optically thick, and as  $R_{out}^{0.58}$  when it is optically thin. Radio emission from CPD Jets or winds may be detectable by ngVLA in future.

We also discuss the radio emission from various CPD models that were constructed to understand the Galilean satellite formation in our solar system. With the “minimum mass sub-nebula” model, ALMA has the sensitivity to detect the CPD if it is 5 AU from the central star. If we use the “gas-starved” disc model, ALMA has enough sensitivity to

detect the CPD if it is 20 AU away from the central star with  $\alpha < 0.01$ .

Although ALMA may have enough sensitivity to detect CPDs, it is difficult to distinguish the unresolved CPDs from the background circumstellar disc. Only if a deep gap/cavity has been carved out or the CPD is far away from the central star, we can distinguish them from the circumstellar disc using ALMA’s highest resolution. The high resolution requirement is where future long baselines array such as the ngVLA would provide the greatest advantage compared to ALMA.

Finally, we find that mm/cm dust particles drift extremely fast in CPDs. Within most of our parameter space, it only takes  $\lesssim 100$ -1000 years for mm dust particles to drift to the central star. The meter barrier in protoplanetary discs becomes the millimetre barrier in circumplanetary discs. Thus, to detect CPDs at radio wavelengths, CPDs need to have a large population of micron-sized dust, a high gas surface density, mechanisms to trap/slow down dust particles, or mechanisms to replenish mm particles efficiently. We have also commented on recent ALMA detection or non-detection of discs around planetary mass objects. Based on the particles’ drift timescale argument, the radio emission may come from micron-sized dust only, or the dust-to-gas mass ratio is significantly smaller than 0.01 in these discs, or the disk has substructures to trap dust particles. These can be tested by future observations.

## ACKNOWLEDGEMENTS

Z.Z. would like to thank Enrique Macias Quevedo, Catherine Espaillat for helpful discussions. The work is stimulated by the discussion of the “Science Use Cases” for ngVLA. Z. Z. acknowledges support from the National Aeronautics and Space Administration through the Astrophysics Theory Program with Grant No. NNX17AK40G. A. I. acknowledges support from the National Aeronautics and Space Administration Grant No. NNX15AB06G.

## REFERENCES

- Andrews S. M., Wilner D. J., Hughes A. M., Qi C., Dullemond C. P., 2009, *ApJ*, **700**, 1502
- Anglada G., Rodríguez L. F., Carrasco-Gonzalez C., 2015, *Advancing Astrophysics with the Square Kilometre Array (AASKA14)*, p. 121
- Ayliffe B. A., Bate M. R., 2009, *MNRAS*, **397**, 657
- Bai X.-N., Stone J. M., 2010, *ApJ*, **722**, 1437
- Bayo A., et al., 2017, *ApJ*, **841**, L11
- Billler B. A., et al., 2014, *ApJ*, **792**, L22
- Boehler Y., Weaver E., Isella A., Ricci L., Grady C., Carpenter J., Perez L., 2017, *ApJ*, **840**, 60
- Bowler B. P., Andrews S. M., Kraus A. L., Ireland M. J., Herczeg G., Ricci L., Carpenter J., Brown M. E., 2015, *ApJ*, **805**, L17
- Calvet N., Gullbring E., 1998, *ApJ*, **509**, 802
- Canup R. M., Ward W. R., 2002, *AJ*, **124**, 3404
- Carrasco-González C., et al., 2016, *ApJ*, **821**, L16
- Currie T., Cloutier R., Brittain S., Grady C., Burrows A., Muto T., Kenyon S. J., Kuchner M. J., 2015, *ApJ*, **814**, L27
- D’Alessio P., Cantó J., Calvet N., Lizano S., 1998, *ApJ*, **500**, 411
- D’Alessio P., Calvet N., Hartmann L., 2001, *ApJ*, **553**, 321
- Espaillat C., et al., 2014, *Protostars and Planets VI*, pp 497–520
- Gressel O., Nelson R. P., Turner N. J., Ziegler U., 2013, *ApJ*, **779**, 59

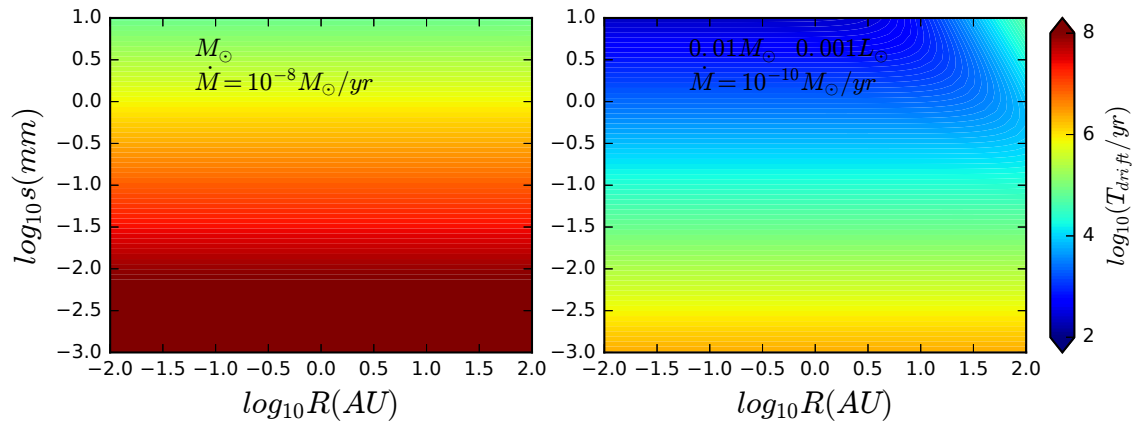


**Figure 9.** The drift timescale for the disc around a solar mass object having  $L = L_{\odot}$  (the left panel) and the disc around a  $0.01 M_{\odot}$  object having  $L = 0.001 L_{\odot}$  (the right panel). In both cases, the disc is irradiation dominated and  $\alpha$  is assumed to be 0.001.

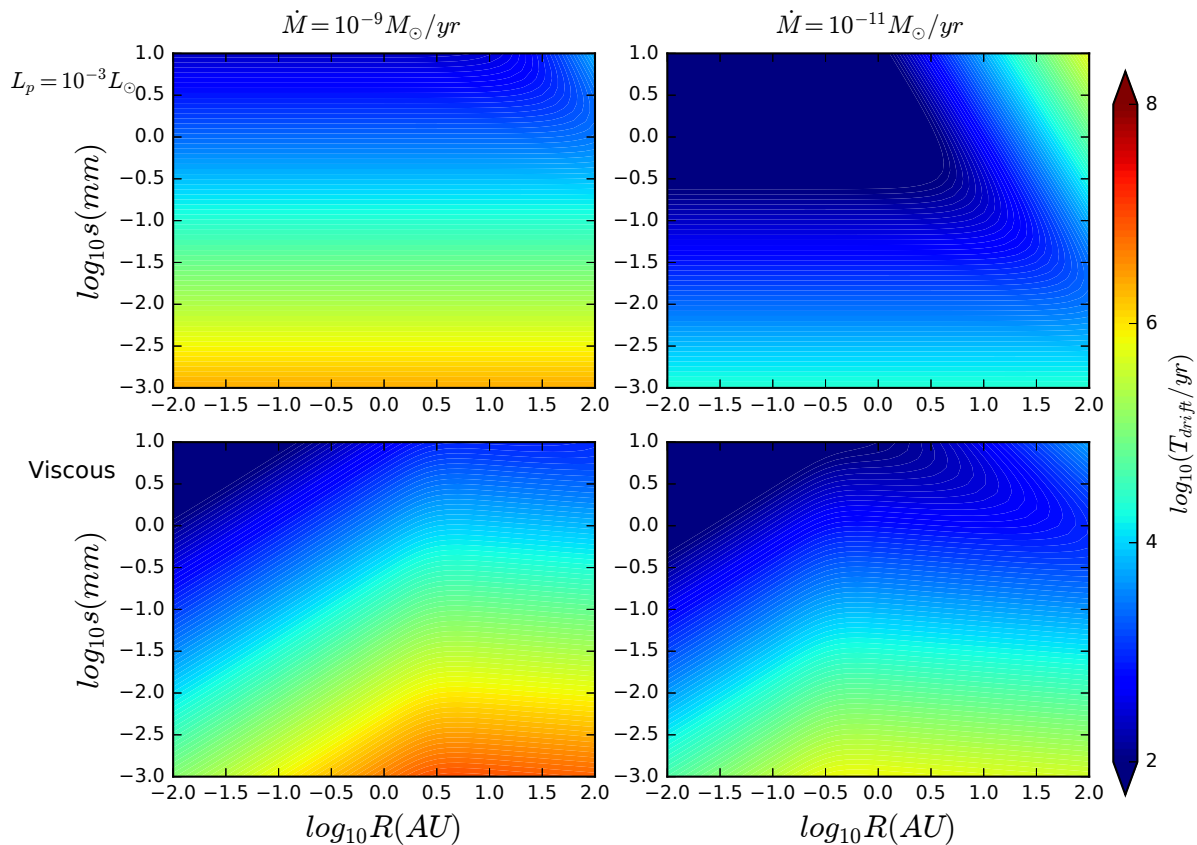


**Figure 10.** The drift timescale for discs around a  $1 M_J$  planet. The discs are either irradiation dominated ( $L_{irr} = 10^{-3} L_{\odot}$ , upper panels) or viscous heating dominated ( $L_{irr} = 0$ , bottom panels. ). Discs that accrete at high and low rates are shown in the left and right panels.

Hubeny I., 1990, *ApJ*, **351**, 632

Isella A., Chandler C. J., Carpenter J. M., Pérez L. M., Ricci L., 2014, *ApJ*, **788**, 129

Kenyon S. J., Hartmann L., 1987, *ApJ*, **323**, 714

Kraus A. L., Ireland M. J., 2012, *ApJ*, **745**, 5

Kraus A. L., Ireland M. J., Cieza L. A., Hinkley S., Dupuy T. J., Bowler B. P., Liu M. C., 2014, *ApJ*, **781**, 20

Kraus A. L., Andrews S. M., Bowler B. P., Herczeg G., Ireland

M. J., Liu M. C., Metchev S., Cruz K. L., 2015, *ApJ*, **798**, L23

Lubow S. H., Seibert M., Artymowicz P., 1999, *ApJ*, **526**, 1001

Lunine J. I., Stevenson D. J., 1982, *ICARUS*, **52**, 14

MacGregor M. A., et al., 2017, *ApJ*, **835**, 17

Marley M. S., Fortney J. J., Hubickyj O., Bodenheimer P., Lissauer J. J., 2007, *ApJ*, **655**, 541

Martin R. G., Lubow S. H., 2011, *MNRAS*, **413**, 1447

Mosqueira I., Estrada P. R., 2003, *ICARUS*, **163**, 198

- Muzerolle J., Hartmann L., Calvet N., 1998, *AJ*, **116**, 455  
Muzerolle J., Calvet N., Hartmann L., 2001, *ApJ*, **550**, 944  
Papaloizou J. C. B., Nelson R. P., 2005, *A&A*, **433**, 247  
Peale S. J., 1999, *ARA&A*, **37**, 533  
Quanz S. P., Amara A., Meyer M. R., Kenworthy M. A., Kasper M., Girard J. H., 2013, *ApJ*, **766**, L1  
Quillen A. C., Trilling D. E., 1998, *ApJ*, **508**, 707  
Rameau J., et al., 2017, *AJ*, **153**, 244  
Reggiani M., et al., 2014, *ApJ*, **792**, L23  
Sallum S., et al., 2015, *Nature*, **527**, 342  
Selina R., Murphy E., 2017, ngVLA Memo # 17,  
Spiegel D. S., Burrows A., 2012, *ApJ*, **745**, 174  
Szulágyi J., Masset F., Lega E., Crida A., Morbidelli A., Guillot T., 2016, *MNRAS*, **460**, 2853  
Takeuchi T., Lin D. N. C., 2002, *ApJ*, **581**, 1344  
Waite J. H., et al., 2017, *Science*, **356**, 155  
Weidenschilling S. J., 1977, *MNRAS*, **180**, 57  
Wolf S. G., et al., 2017, preprint, ([arXiv:1705.08470](https://arxiv.org/abs/1705.08470))  
Wu Y.-L., et al., 2017, *ApJ*, **836**, 223  
Youdin A. N., Goodman J., 2005, *ApJ*, **620**, 459  
Zhou Y., Herczeg G. J., Kraus A. L., Metchev S., Cruz K. L., 2014, *ApJ*, **783**, L17  
Zhu Z., 2015, *ApJ*, **799**, 16  
Zhu Z., Ju W., Stone J. M., 2016, *ApJ*, **832**, 193

This paper has been typeset from a  $\text{\TeX}/\text{\LaTeX}$  file prepared by the author.